Cape Peninsula University of Technology

Numerical Optimisation of Electron Beam Physical Vapor Deposition Coatings for Arbitrarily Shaped Surfaces

Dissertation

Submitted in Fulfillment of the Requirements for the Degree:

MAGISTER TECHNOLOGIAE

In

MECHANICAL ENGINEERING

Name	:	**Marouen**
Surname	:	**Mahfoudhi**
Student Number	:	**213245701**
Supervisor	:	**Dr Nawaz Mahomed**

Table of Contents

List of Figures

List of Tables

1. Introduction

1.1 Rationale

For the last few decades, methods to improve the engine efficiency and reduce the fuel consumption of jet engines have received increased attention. One of the solutions is to increase the operating temperature in order to increase the exhaust gas temperature, resulting in an increased engine power.

However, this approach can be degrading for some engine parts such as turbine blades, which are required to operate in a very hostile environment (at ≈ 90% of their melting point temperature).

Thus, an additional treatment must be carried out to protect these parts from corrosion, oxidation and erosion, as well as to maintain the substrate's mechanical properties which can be modified by the high temperatures to which these parts are exposed.

Coating, as the most known protection method, has been used for the last few decades to protect aircraft engine parts. According to Wolfe and Co-workers [1], 75% of all engine components are now coated. The most promising studies show that the thermal barrier coating (TBC) is the best adapted coating system for these high temperature applications.

TBC is defined as a fine layer of material (generally ceramic or metallic material or both) directly deposited on the surface of the part In order to create a separation between the substrate and the environment to reduce the effect of the temperature aggression.

However, the application of TBCs on surfaces of components presents a challenge in terms of the consistency of the thickness of the layer. This is due to the nature of the processes used to apply these coatings. It has been found that variations in the coating thickness can affect the thermodynamic performance of turbine blades as well as lead to premature damage due to higher thermal gradients in certain sections of the blade. Thus, it is necessary to optimise the thickness distribution of the coating.

1.2 Problem Statement

The most critical part of the turbine blade manufacture process is the thermal barrier coating (TBC) system. This consists of two layers: a bond coat for corrosion resistance and a ceramic topcoat for heat protection. These coatings are applied using an EB-PVD (Electron Beam Physical Vapor Deposition) system.

One of the critical aspects of TBCs is the consistency in the layer thickness.

Certain researchers have developed techniques to control the coating thickness of EB-PVD systems. These techniques have been studied and analysed. However, there are shortcomings in these techniques in that they do not solve the problem of equalising the thickness distribution along surfaces to be coated.

1.3 Objectives and Methodology

In this research project, the main objective is to develop a numerical technique for controlling the thickness of EB-PVD coatings on arbitrarily-shaped substrates. The technique will be based on the numerical solution of certain established coating distribution laws. This will require solving certain numerical parameters based on experimental comparisons, which is necessary for the numerical prediction of coating thickness distribution on rotating parts of arbitrary shape.

The methodology applied in this research is as explained in the graphic below.

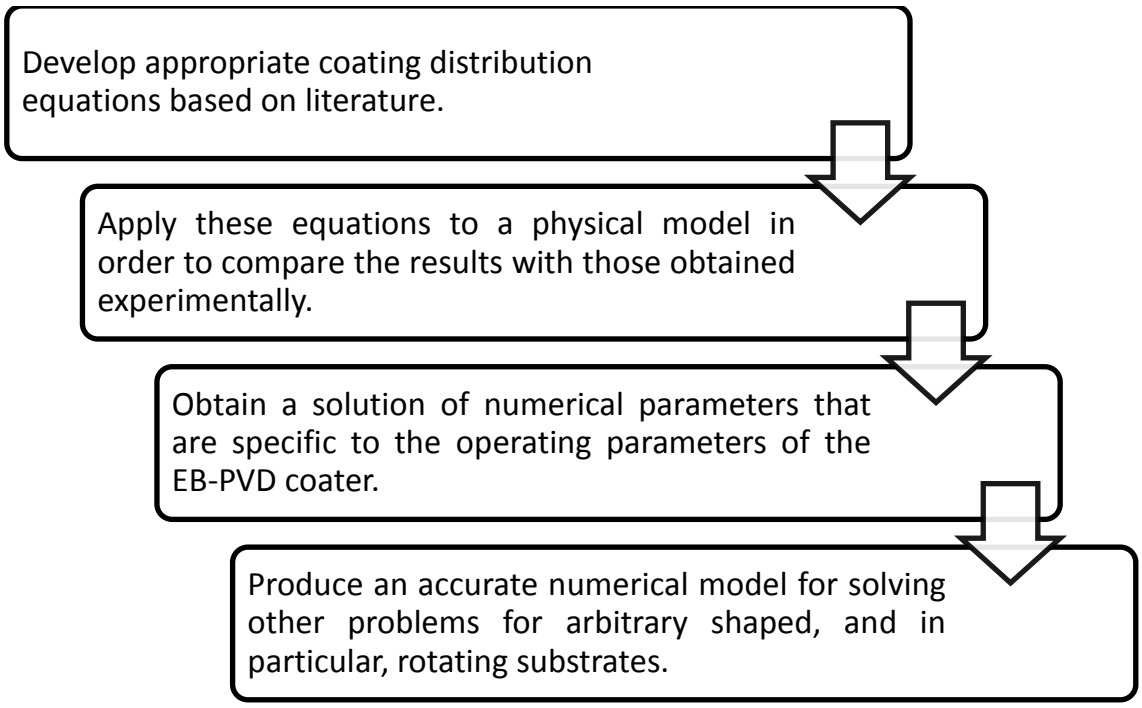

Figure 1: The methodology followed in this research.

It will be proposed that future work could entail a numerical solution based on the minimisation of a thickness functional using a finite element approach.

This research project will be conducted in the Faculty of Engineering at CPUT in cooperation with the Laboratory for Aerospace Materials at Rzeszow University of Technology.

The EB-PVD coating system at Rzeszow University of Technology (PRZ) will be used to conduct experimental trials for coating thickness distribution. In addition, certain specialised equipment at PRZ will be used to measure the thickness of coated surfaces.

2. Literature Review

2.1 EB-PVD Coating Process

EB-PVD is a coating process which uses an electron-beam as a heat source to evaporate a ceramic or metallic ingot.

The generation of the beam takes place in an electron gun. The principal used is the thermo-ionic emission of free electrons from a heated metal filament. The electrons are then shaped into a beam using an electrostatic field.

The ingot loaded into the coating machine is bombarded by the electrons using an electromagnetic field to create a vapor plume in which the substrate is placed (Figure 2).

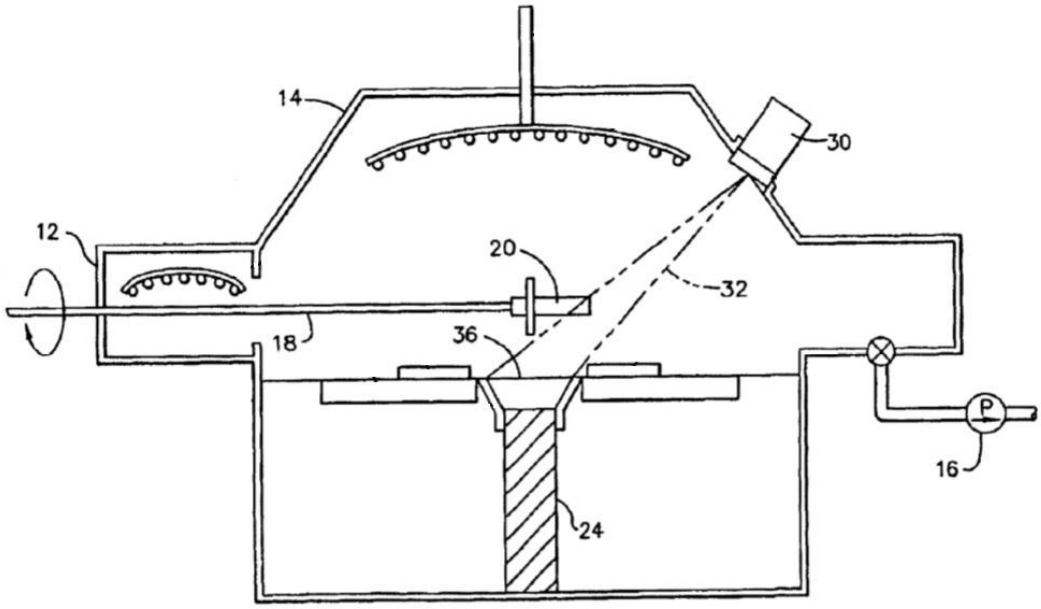

Figure 2: Schematic for an EB-PVD coating chamber (EB-PVD technical documentation, R&D Laboratory for Aerospace Materials, Rzeszow University of Technology).

Those particles (evaporated material) will be deposited on the substrate surface creating a thermal barrier to protect the coated part from external aggressions such as hot corrosion.

The whole EB-PVD coating process is conducted under a high vacuum (10^{-4} to 10^{-6}Pa).

The EB-PVD coater (from ALD Technologies) at the Laboratory for Aerospace Materials. On the left is the control system for controlling the coating parameters in the coating chamber, the latter shown open on the right. The white ceramic ingots are visible, which are loaded into the gun barrel and bombarded with an electron beam to create a plasma plume of the ceramic material. The plume is then allowed to travel onto the blades, forming the thermal barrier coating.

The bottom left shows the actuator mechanism in the loading chamber. Three rotating holders are visible for mounting the blades. Once the blades are mounted, the actuator is moved to the right into the coating chamber, all under vacuum of 10^{-4} to 10^{-6} Pa (depending on the application).

Figure 3: The EB-PVD coater (from ALD Technologies).

The Electron Beam Physical Vapor Deposition coating method can be used in many different applications. The most well-known application of the EB-PVD process is the application of heat-resistant, multi-layered coatings for aircraft parts and industrial turbine blades exposed to high temperatures and aggressive environments.

This process is also used for cutting tools to increase the useful lifetime by making them more resistant to oxidation. The application of thin films of ZrO_2, TiO_2 and HfO_2 for high performance solar cells as well as high precision sensors is also frequent.

The main characteristic of this process is the longer lifespan of rotating parts under severe conditions. Lugscheider et al [2] showed that coated parts using the EB-PVD process have 10 times more cycles than parts coated with another process. This is due to the columnar structure of the EB-PVD coating (Figures 4 and 5), which is strain-tolerant.

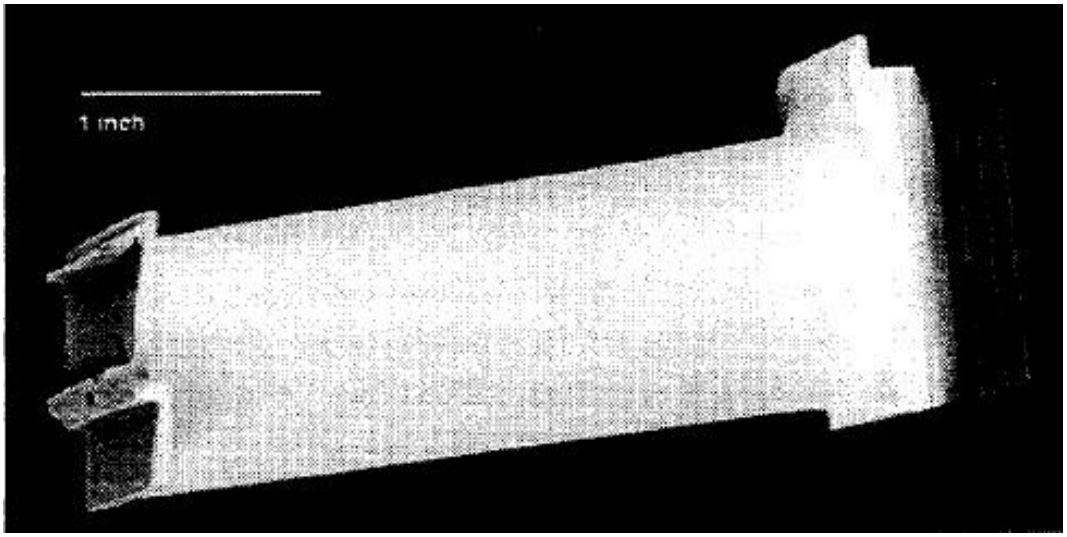

Figure 4: Turbine blade.

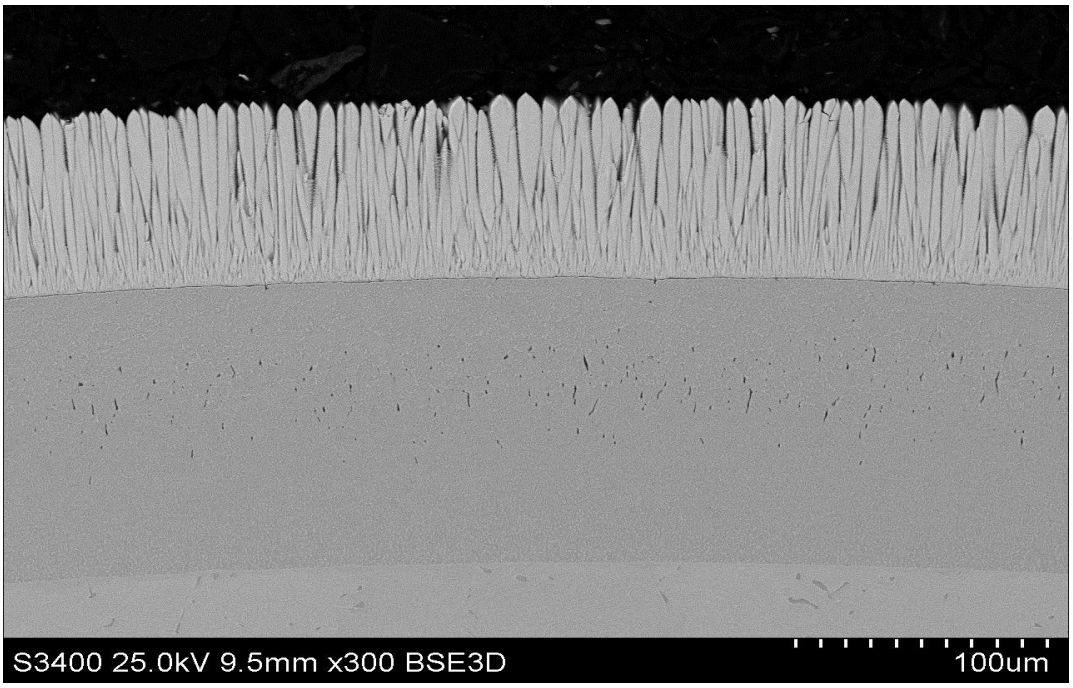

Figure 5: SEM Micrograph of a coated surface showing the columnar microstructure of a turbine blade coated with EB-PVD TBC.

The same research proved, after a comparison of 2 types of heating methods, electron-beam gun as a direct heating source and radiation heater as an indirect source, that EB-PVD is superior. This is due to the presence of equiaxed crystals with small diameters in the microstructure, which is very important in order to protect the part from thermal shock.

Another advantage of EB-PVD is that, in comparison with the plasma spray coating process, the electron beam is much smoother (1.4µm to 1.5µm) as opposed to plasma spray (5µm).

In the case of coating parts that cannot be exposed to excessive temperatures, EB-PVD is preferred over other processes such as chemical vapor deposition coating (CVD) which is a high-temperature process.

The characteristics of the electron beam vapor deposition coating process are not only technical but also economical as there is a possibility to coat many parts at the same time, decreasing the cost per part.

2.2 Coating Thickness Control

The electron beam physical vapor deposition process for TBCs is very complex. At the same time, it is also very useful in order to increase the efficiency of the parts exposed to hostile environments, and hence the need to master all the aspects of this process.

For this reason, a number of research projects were conducted to predict and control the coating film thickness, taking into account different parameters such as the inclination of the substrate surface relative to the horizontal plane, the focus of the vapor flux and the shape of the work-piece.

The utilisation of different components may require different coating film thickness distributions. For a stationary part exposed to a high temperature, a uniform thickness is preferable. On the other hand, for rotating parts like turbine blades, a regular coating thickness would degrade the aerodynamics performance, and there is a need to limit the thickness in the trailing edge. In 1998, Pereira et al undertook research to predict the deposition rate and the columnar inclination using one ideal source [3].

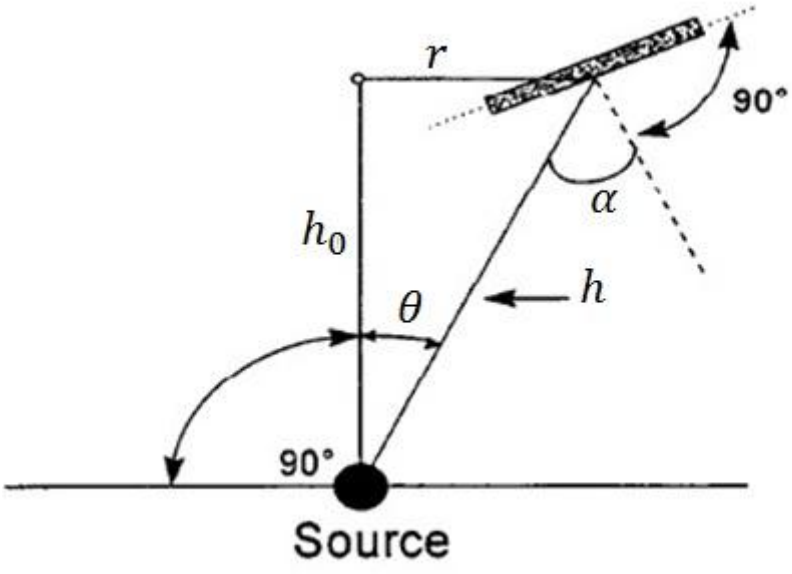

Figure 6: Schematic representation of an ideal point source evaporator.

According to Pereira [3], the thickness of the coating film follows an inverse square law.

$$\frac{d_s}{d_0} = \frac{h_0^2}{h^2} cos(\theta)^n \, cos(\alpha) \quad (1)$$

where d_s is the thickness in the point at the distance h of the vapor source, d_0 is the thickness directly above the source at a distance h_0, and α, θ and n define the source to substrate geometry and the evaporation characteristics of the source (see Figure 6).

The following graph shows clearly the effect of the index n on the deposition rate using a constant height of the substrate measured directly above the source ($h = 25\ cm$). The author used three random values of n (1, 5 and 9) for the thickness prediction calculation using the equation 1 presented above. It has been observed that as the parameter n is increased, the vapor plume becomes more focused in the centre (see Figure 12) and the thickness is less important on both sides of the substrate (see Figure 7).

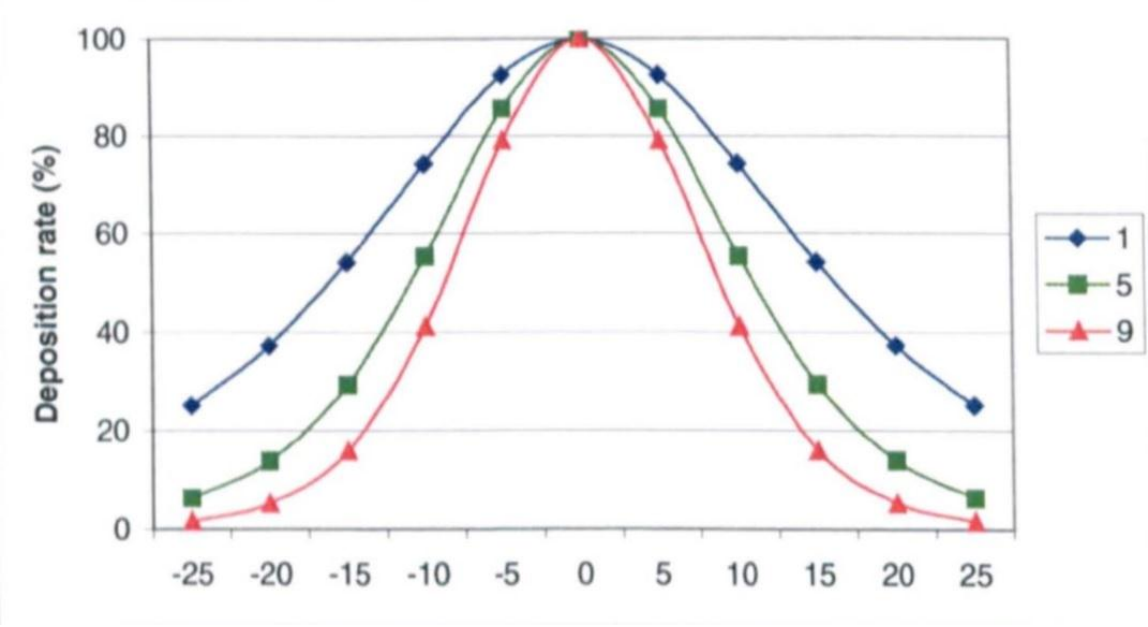

Figure 7: Predicted deposition rate along the centreline with index $n = 1,\ 5$ and 9.

Another important parameter that influences the deposition profile as well as the value of the thickness is the distance h. As is noticeable in Figure 8, the deposition profile changes according to the height of the substrate above the source. This figure does not show the effect on the values of the thickness, simply because the thickness at the centre point is kept equal to 100% for the three cases to emphasize the effect on the deposition distribution. In Figure 9, the influence of the height on the thickness values is clearly shown; the thickness values increase as the distance between the source and the substrate decreases.

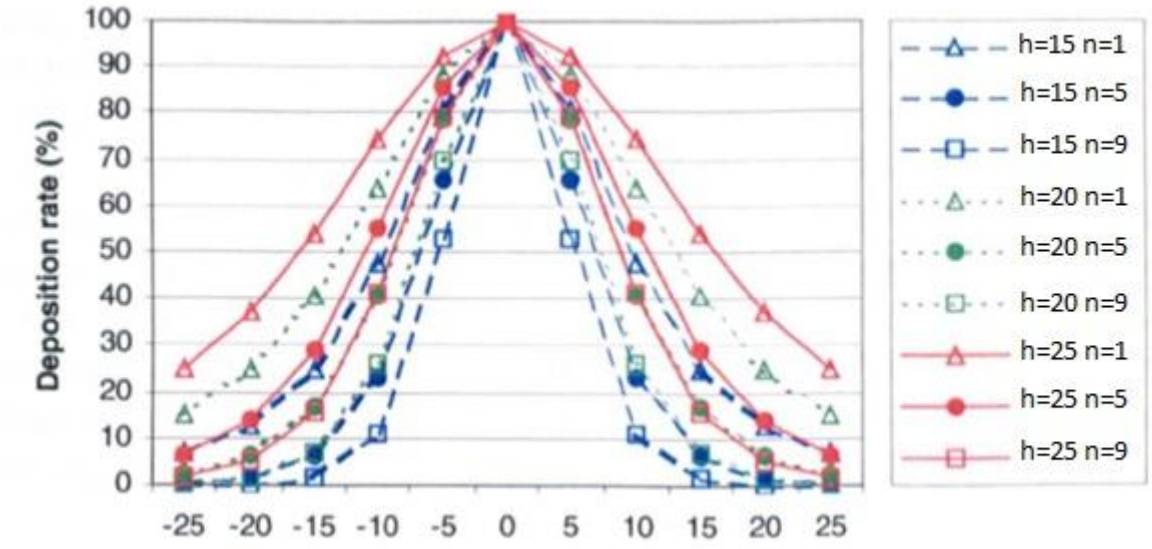

Figure 8: Predicted deposition rate for 3 different heights along the centreline (the thickness in the centre point d_0 is considered as 100% for all the heights).

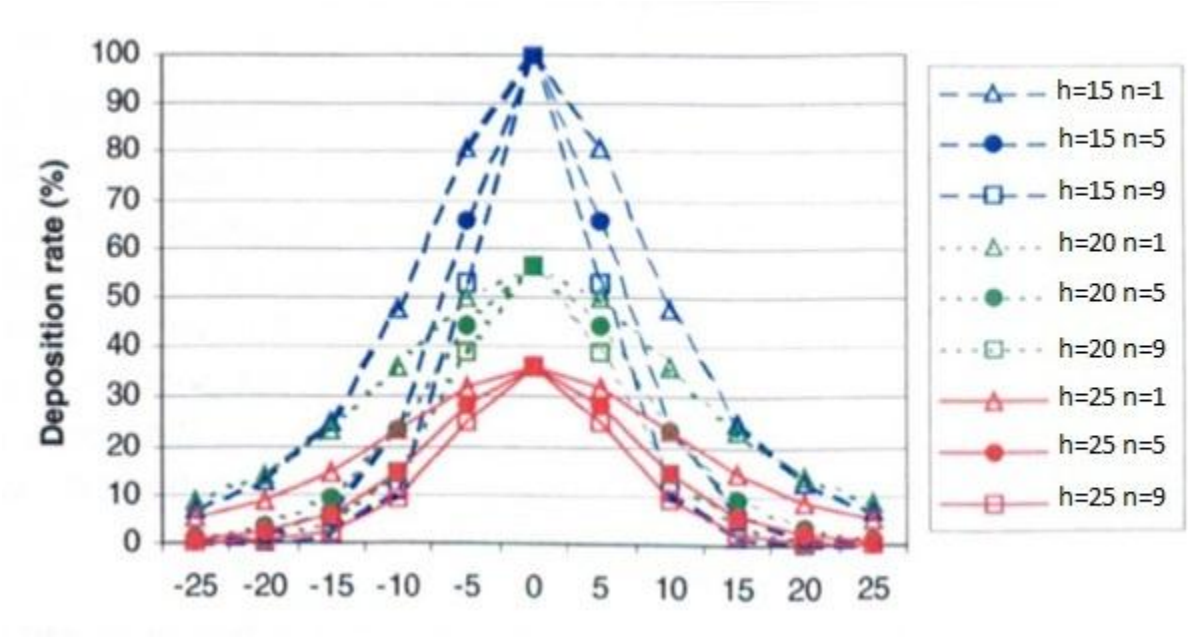

Figure 9: Predicted deposition rate for 3 different heights along the centreline ($h = 15,\ d_0 = 100$; $h = 20,\ d_0 = 56.25$; $h = 25, d_0 = 36$).

Finally, the last aspect that Pereira considered in his research is the angle of inclination between the substrate and the horizontal plan. Five different angles were used as represented in Figure 10.

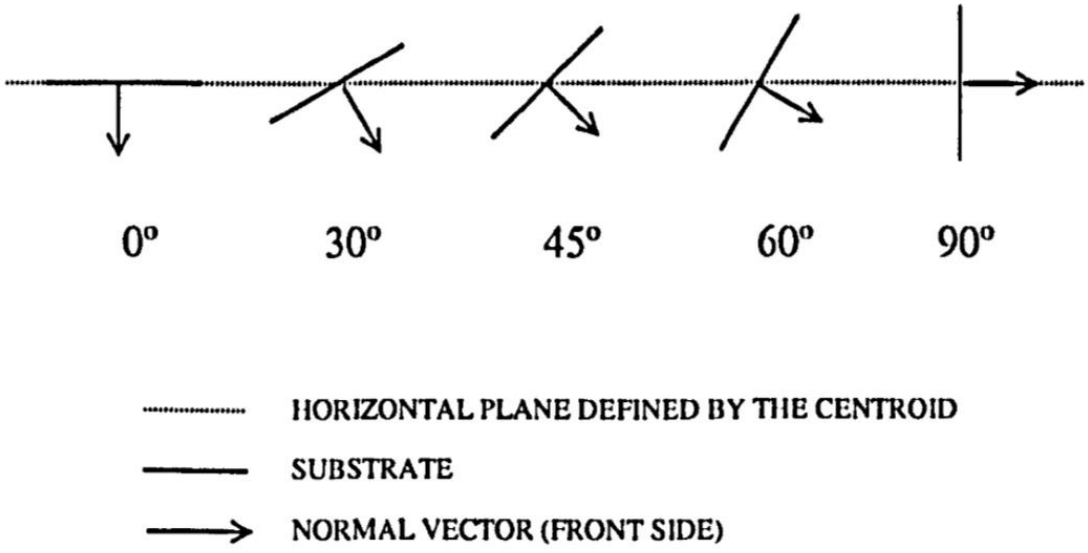

Figure 10: The different configurations used.

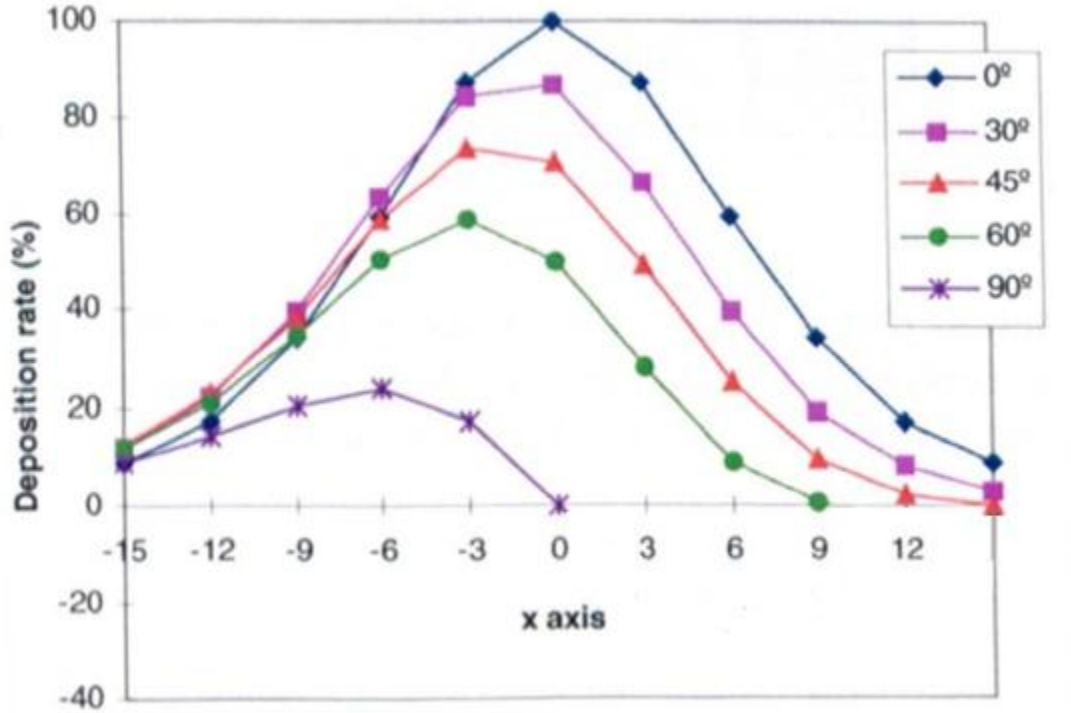

Figure 11: Deposition rate along the centreline for the five different inclinations $h = 15,\ n = 5$.

According to these results (Figure 11), it is clear that the coating film thickness is more pronounced when the substrate is directly above the source and at the horizontal configuration (inclination angles θ and α are equal to 0).

The negative thickness in the graph indicates a deposition on the rear side of the sample, so the actual thickness is its absolute value. These results are very important, but there is a shortcoming; this model deals only with simple geometry (stationary flat plate) which might not be applicable for complex geometries, such as in the case of turbine blades.

In trying to overcome this limitation, Indraneel et al [4] developed another model using a different approach. In this case, a cosine model is used for modelling the shape of the vapor plume generated in EB-PVD, and the vapor intensity can be expressed by the following equation:

$$I(\alpha) = I_0 \cos(\alpha)^n \qquad [kg/m^2 s] \tag{2}$$

where $I(\alpha)$ is the vapor intensity in the substrate surface located in direction α degrees from the normal to the vapor-emitting surface, n is a parameter depending on the rate of evaporation and I_0 is the intensity in the vertical direction directly above the source where α is equal to 0. It can be clearly seen that, in this case, the maximum intensity is obtained. Following the same reasoning, it is approximated that the vapor plume has the same shape as the intensity, thus, it can be expressed as:

$$r(\alpha) = r_0 \cos(\alpha)^n \qquad [m] \tag{3}$$

where $r(\alpha)$ is the range of vapor plume in a direction α degrees from the normal to the vapor-emitting surface, and r_0 is the range of the vapor plume in the vertical direction for $\alpha = 0$ and equal to h_v, as shown in Figure 12 below.

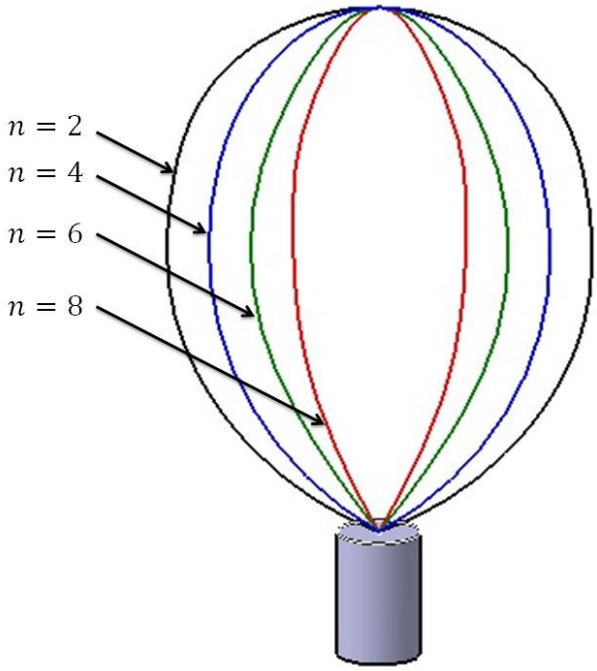

Figure 12: Vapor plume shape.

For a stationary flat plate, the coating film thickness has been modelled as follows [4]:

$$\frac{d_s}{d_{s_0}} = \frac{1}{\left(1+\left(\frac{r_s}{h_v}\right)^2\right)^{\frac{n+3}{2}}} \quad (4)$$

Based on Equation 4, Indraneel et al [4] developed a new equation for the coating film thickness for a cylindrical shaped substrate.

$$d_s = d_{s_0}\left[\frac{\left(h_v^2+cos(\alpha)^2\right)}{(h_v+h')^2}\right] cos(\alpha+\theta)\, cos(\alpha)^n \quad (5)$$

According to the results, it can be seen that the coating thickness distribution varies inversely with respect to the angle α and the distance between the vapor source and the substrate (Figure 13).

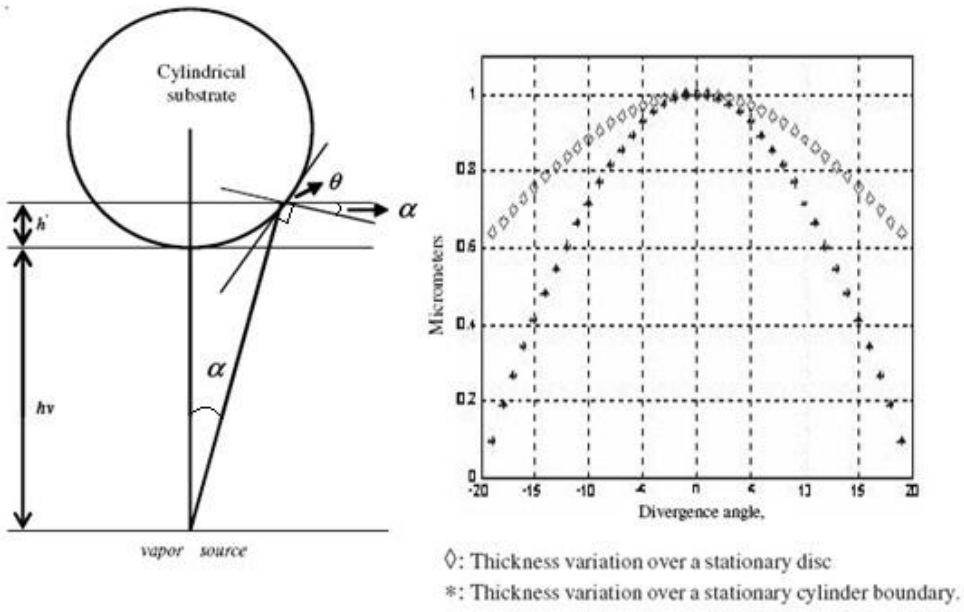

Figure 13: Schematic representation of the coating process of a cylindrical shaped substrate and the thickness results [4].

A comparison between the experimental results and the predicted coating thicknesses shows a good match with a maximum error of 13.15% for the flat plate and 10.70% for the cylindrical substrate as shown in the tables below (Tables 1 and 2).

Table 1: Comparison of experimental and predicted coating film thicknesses for a flat plate substrate [4].

Case Number 1	Divergence Angle α	Experimental $\frac{d_s}{d_{s_0}}$	Predicted $\frac{d_s}{d_{s_0}}$	Difference %
Titanium (Ti)	13.60	0.933	0.892	4.54%
	25.86	0.733	0.660	11.10%
	13.60	0.954	0.892	6.92%
	25.86	0.746	0.660	13.15%
	13.60	0.869	0.892	2.57%
	25.86	0.700	0.660	6%

Table 2: Comparison of experimental and predicted coating film thicknesses for a cylindrical substrate.

Case Number 2	Divergence Angle α	Experimental $\frac{d_s}{d_{s_0}}$	Predicted $\frac{d_s}{d_{s_0}}$	Difference %
Tungsten (W)	19.19	0.025	0.023	8%
	25.80	0.020	0.019	5%
	-30.26	0.014	0.016	10.70%
	31.66	0.014	0.015	7.10%

A number of experiments and models were applied to solve and ameliorate the prediction of the coating thickness. One of these [5] involves a comparison of experimental measurements and analytical results using a new model: the Knudsen's cosine law of emission.

This law states that the coating thickness for a cylindrical substrate can be calculated using the following equation.

$$d_s = \frac{M_e}{\rho_{coating}} \left(\frac{cos(\theta)\, cos(\varphi)}{\pi r^2} \right) \tag{6}$$

where d_s is the coating thickness, M_e is the mass evaporated, $\rho_{coating}$ is the density of coating, r is the distance between the source and the receiving surface and θ and φ are the geometrical angles defining the position of the substrate as shown in the following figure (Figure 14).

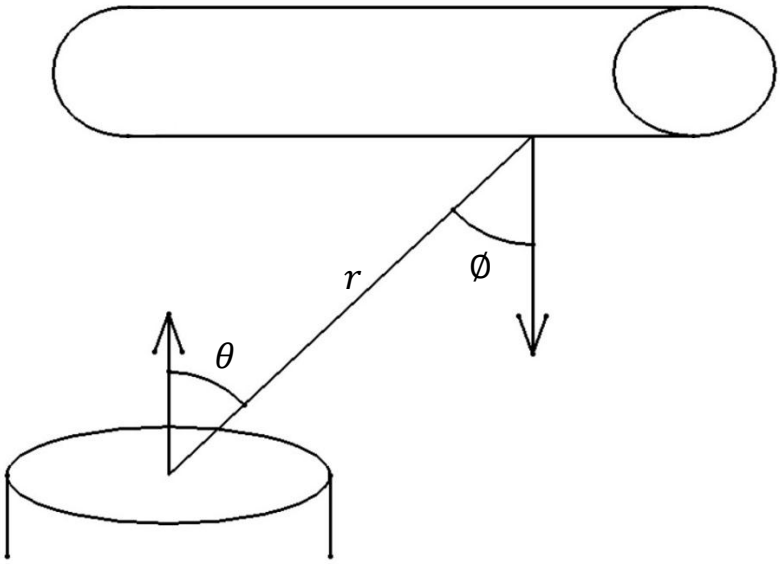

Figure 14: Schematic representation of the coating process of a cylindrical shaped substrate.

The experimental procedure was simple: a cylindrical rod was positioned above two point sources at different heights (Figure 15) and, after the coating process, measurements were taken and compared to the predicted results.

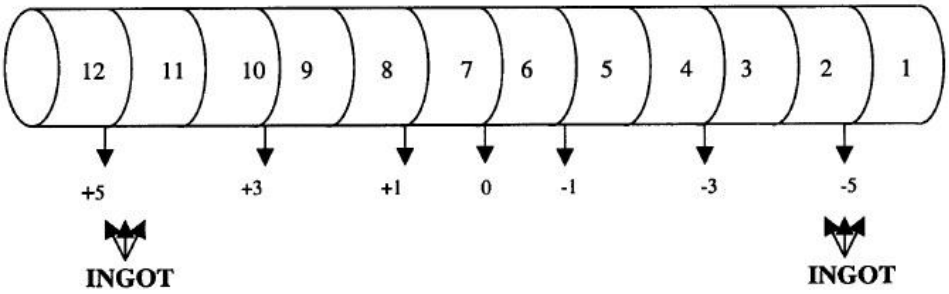

Figure 15: Cylinder sections.

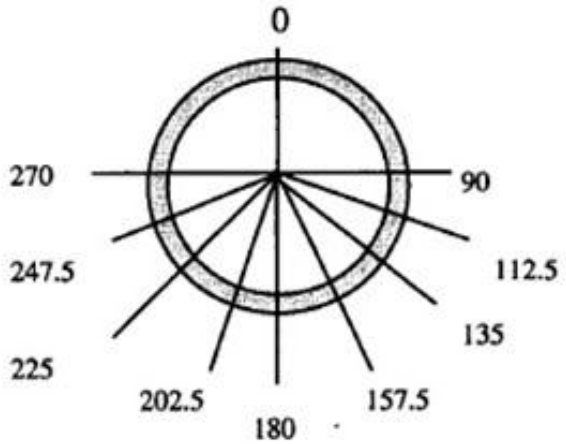

Figure 16: Marked angular position on the cross section of the cylinder.

The results show how the thickness varies from the predicted ones as a function of the angle (Figure 16) for a given height (baseline + 0.0142 m) (Figure 17).

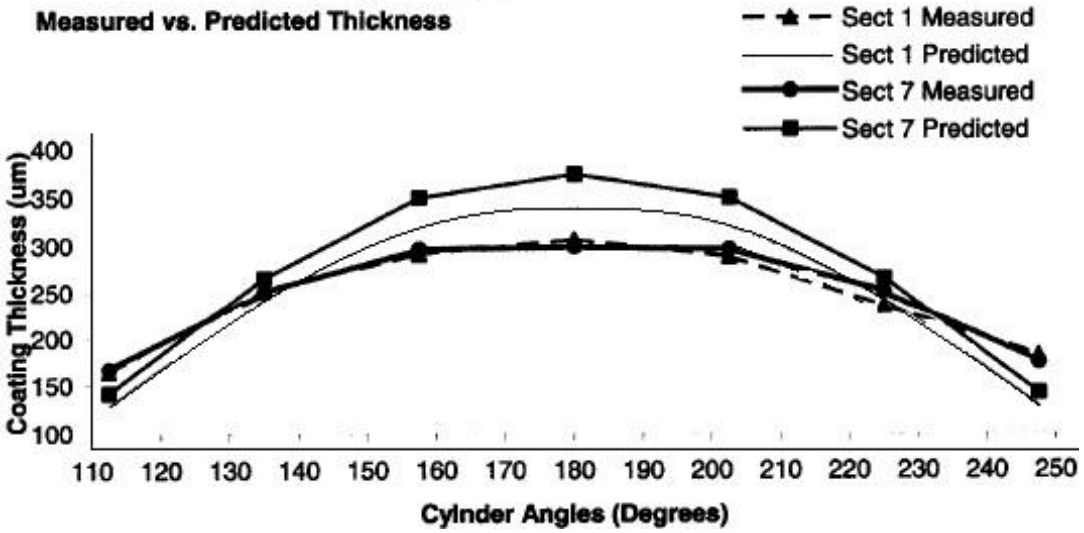

Figure 17: Measured versus predicted thickness.

It has been noticed that this model does not take into account n which is a parameter depending on the rate of evaporation, or the focus of the vapor plume. In 2009, S. Baek and V. Prabhu [6] introduced this parameter into the Knudsen's cosine law model, and the equation of the coating thickness became:

$$d_s = \frac{m}{\rho}\frac{n+1}{2}\frac{cos(\varphi)^n\, cos(\theta)}{\pi r^2} \tag{7}$$

where m is the mass evaporated, ρ is the material density, n the parameter depending on the rate of evaporation, r the distance between the source and the coated surface on the substrate, and φ and θ are the geometrical angles defining the position of the cylinder with respect of the vapor source.

2.3 Conclusion

During the past three decades, a number of researchers have attempted to solve the coating film thickness problem. Each of these efforts brought a new model for the prediction of the coating thickness. However, none of these models were applied to arbitrarily shaped and rotating substrates, and are valid for particular defined surface geometries only. The purpose of this study is to develop a model, taking into account a maximum number of parameters, first by solving the parameter n (which depends on the rate of evaporation) using experimental results, and then to substitute the value of n into the thickness equation to control the coating thickness for rotating substrates with complex geometry.

3. Mathematical Model

3.1 Knudsen's Law of Emission

The direction in which a molecule rebounds from a solid wall is independent of the direction in which it approaches the wall and is governed by the cosine law: the probability P_s that a molecule leaves the surface in the solid angle $d\omega$ forming an angle γ with the normal to the surface is (see Figure 18), given by:

$$P_s = \frac{d\omega}{\pi} cos(\gamma) \tag{8}$$

This is known as Knudsen's law of emission. This law expresses the probability P_s as a function of the angle γ and the solid angle $d\omega$.

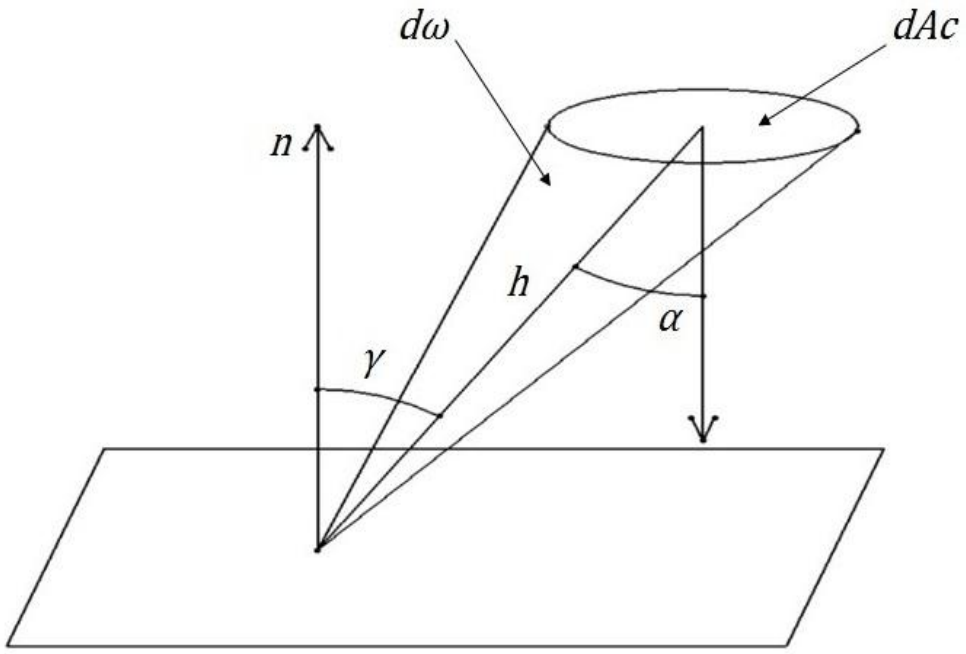

Figure 18: Figure representing the Knudsen's law of emission.

At the same time, the probability P_s can also be expressed in terms of the ratio between the mass of ceramic material deposited and the total mass evaporated from the ingot source:

$$P_s = \frac{dM_e}{M_e} \tag{9}$$

where M_e is the total mass of the evaporated material.

The elementary area upon which the evaporated material is condensed, as shown in Figure 18, is given by:

$$dA_c = \frac{h^2 d\omega}{cos(\alpha)} \tag{10}$$

where h is the distance separating the source from the targeted point. In order to find an expression of the solid angle $d\omega$, the Equation 10 can be rewritten as:

$$d\omega = \frac{dA_c\, cos(\alpha)}{h^2} \tag{11}$$

By substituting Equation 11 and Equation 9 in the Knudsen's law equation (Equation 8), the following equation is obtained:

$$P_s = \frac{dM_e}{M_e} = \frac{dA_c\, cos(\alpha)}{\pi\, h^2} cos(\gamma) \tag{12}$$

After simplifying Equation 12, the expression of the mass deposited dM_e is obtained as:

$$dM_e = \frac{M_e\, dA_c\, cos(\alpha)}{\pi\, h^2} cos(\gamma) \tag{13}$$

Dividing both sides of Equation 13 by the density ρ of the evaporated material then gives:

$$\frac{dM_e}{\rho} = \frac{M_e}{\rho} \frac{dA_c\, cos(\alpha)}{\pi\, h^2} cos(\gamma) \tag{14}$$

In effect, an equation function of the volume deposited has been obtained:

$$dV_e = \frac{M_e}{\rho} \frac{dA_c\, cos(\alpha)}{\pi\, h^2} cos(\gamma) \tag{15}$$

where V_e is the total volume evaporated.

In order to find an equation to calculate the coating thickness, Equation 15 is divided by the area dA_c which gives the thickness d_s:

$$d_s = \frac{M_e}{\rho} \frac{cos(\alpha)}{\pi\, h^2} cos(\gamma) \tag{16}$$

According to literature [6], a parameter n is introduced into the thickness equation; this parameter is dependent on the rate of evaporation.

Thus, the final model can be expressed as:

$$d_s = \frac{M_e}{\rho}\frac{cos(\alpha)}{\pi\, h^2} cos(\gamma)^n \left(\frac{n+1}{2}\right) \quad (17)$$

where d_s is the coating thickness, M_e is the total mass evaporated, h is the distance between the vapor source and the targeted point, n is the rate of evaporation parameter and the angles γ and α as shown in Figure 18.

3.2 Inverse Square Law for Coating Thickness Prediction

According to Pereira [3], the thickness of the coating film follows an inverse square law as shown below in Equation 18.

$$\frac{d_s}{d_0} = \frac{h_0^2}{h^2} cos(\gamma)^n\, cos(\alpha) \quad (18)$$

where d_0 is the thickness directly above the source. The following demonstration shows how the Equation 18 can be obtained using the model demonstrated earlier in Section 3.1 (Equation 17).

Just above the source, both angles α and γ are equal to 0, so the Equation 17 becomes

$$d_0 = \frac{M_e}{\rho\, \pi\, h_0^2} \left(\frac{n+1}{2}\right) \quad (19)$$

Thus, dividing the expression of d_s (Equation 17) by d_0 which is the thickness just above the source gives the following Equation 20:

$$\frac{d_s}{d_0} = \frac{\frac{M_e}{\rho}\frac{cos(\alpha)}{\pi\, h^2} cos(\gamma)^n \left(\frac{n+1}{2}\right)}{\frac{M_e}{\rho\, \pi\, h_0^2}\left(\frac{n+1}{2}\right)} \quad (20)$$

After simplification of the Equation 20, the inverse square law equation presented is similarly obtained:

$$\frac{d_s}{d_0} = \frac{h_0^2}{h^2} cos(\gamma)^n\, cos(\alpha) \quad (21)$$

The aforementioned analysis demonstrates that the inverse square law equation to predict the coating thickness is based on the same Knudsen's law of emission that was presented in Section 3.1 (Equation 17).

3.3 Flat Plate Shaped Substrate

In this section, another form of the inverse square law will be demonstrated. This new form of the Equation 21 is used in the particular case of a static flat plate shaped substrate as shown in Figure 19 below.

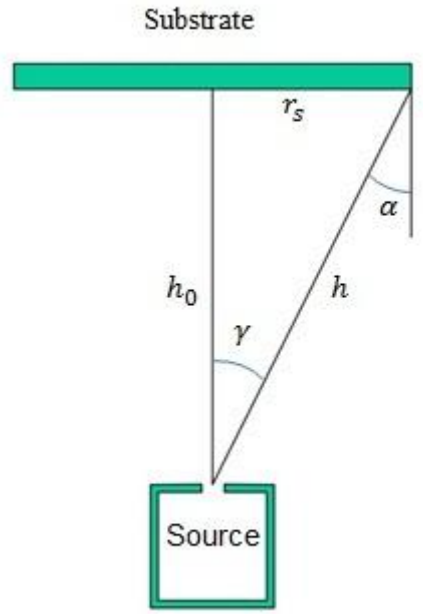

Figure 19: Figure representing a flat plate shaped substrate.

It is clearly noticeable that, since the substrate is placed horizontally at a distance h_0 above the vapor source, the two angles α and γ are equal. The purpose is to rewrite the inverse square law (Equation 21) as a function of distances only by using simple trigonometric formulae.

The distance h separating the source from the point of interest where the thickness will be calculated can be expressed using the other two edges of the triangle as follows:

$$h^2 = h_0^2 + r_s^2 \tag{22}$$

Substituting Equation 22 into the inverse square law given by Equation 21 results in:

$$\frac{d_s}{d_0} = \frac{h_0^2}{h_0^2 + r_s^2} cos(\gamma)^n \, cos(\alpha) \tag{23}$$

However, in the case of a flat plate, γ and α are equal. Equation 23 therefore reduces to:

$$\frac{d_s}{d_0} = \frac{h_0^2}{h_0^2+r_s^2} cos(\gamma)^{n+1} \quad (24)$$

Alternatively, it can be written as follows:

$$\Leftrightarrow \frac{d_s}{d_0} = \frac{h_0^2}{h_0^2+r_s^2} (cos(\gamma)^2)^{\frac{n+1}{2}}$$

$$\Leftrightarrow \frac{d_s}{d_0} = \frac{h_0^2}{h_0^2+r_s^2} \left(\frac{h_0^2}{h^2}\right)^{\frac{n+1}{2}}$$

$$\Leftrightarrow \frac{d_s}{d_0} = \frac{h_0^2}{h_0^2+r_s^2} \left(\frac{h_0^2}{h_0^2+r_s^2}\right)^{\frac{n+1}{2}}$$

$$\Leftrightarrow \frac{d_s}{d_0} = \left(\frac{h_0^2}{h_0^2+r_s^2}\right)^{\frac{n+3}{2}} \quad (25)$$

By simplifying Equation 25 by h_0^2 gives the desired form as shown below:

$$\frac{d_s}{d_0} = \frac{1}{\left(1+\left(\frac{r_s}{h_0}\right)^2\right)^{\frac{n+3}{2}}} \quad (26)$$

In conclusion, the two different forms of the inverse square law demonstrated in Equation 21 and Equation 26 both result from Knudsen's law of emission (Equation 17). Hence, the latter can be considered as the general form of the coating thickness equation. In this study, Equation 17 will be used in order to calculate the coating thickness for different substrates.

3.4 A Numerical Optimisation Model for Coating Thickness Distribution

Predicting the coating thickness is very important for a better understanding of the coating process, furthermore, it is essential for the optimisation problem which is considered as a big challenge for the industry.

Indeed, due to the nature of the coating process used in the industry, it is very difficult to obtain an equal thickness across the substrate surface, particularly when the shape of the coated part is complex.

This heterogeneity of the thickness can create various problems during the use of the part. For instance, a difference in the coating thickness for turbine blades can affect the aerodynamic behaviour of the part by changing the original shape designed for an optimal working condition (penetration in the air, vibrations…).

In addition, the lifespan of the coated part can be affected, in fact, the substrate is exposed to a very hostile environment and the variation of the coating thickness can cause a temperature gradient in the part, resulting in deformation as well as exposing certain areas of the substrate to corrosion. Consequently, the part will undergo premature degradation.

In this section, a numerical model will be developed in order to equalise the coating thickness across the substrate surface. This model will be based on the mathematical model demonstrated earlier (Equation 17). The model involves the variation of the rotation velocity with respect to time during the coating process.

The Knudsen's Law of Emission given previously in Equation 17:

$$d_s = \frac{M_e}{\rho}\frac{cos(\alpha)}{\pi\, h^2} cos(\gamma)^n \left(\frac{n+1}{2}\right) \tag{17}$$

where d_s is the thickness calculated in the point of interest at time t, will be used to develop a minimisation functional for the coating thickness distribution.

To calculate the thickness in a certain elementary surface $d\Gamma$ during the whole process, integration over time is necessary, giving the integral:

$$\int_0^T \frac{m_e}{\rho}\frac{cos\big(\alpha(x,t)\big)}{\pi\, h(x,t)^2} cos\big(\gamma(x,t)\big)^n \left(\frac{n+1}{2}\right) dt \tag{27}$$

where m_e the mass is evaporated per second and T is the total process time. This gives the total thickness at a certain point on the substrate. To calculate the coating distribution over the whole surface of the substrate D_s, an integration over the domain Γ is required (see Figure 20).

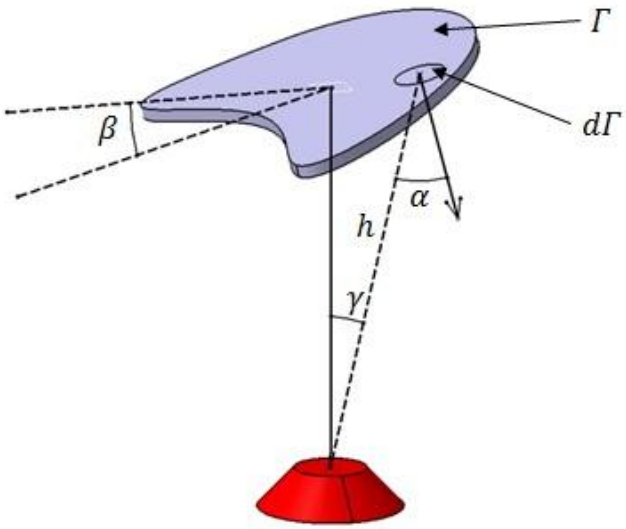

Figure 20: Configuration of an arbitrarily-shaped substrate.

$$D_S = \int_\Gamma \left[\int_0^T \frac{m_e}{\rho} \frac{cos(\alpha(x,t))}{\pi\, h(x,t)^2} cos(\gamma(x,t))^n \left(\frac{n+1}{2}\right) dt \right] d\Gamma \quad (28)$$

The variation in coating thickness is then minimised across the domain, resulting in the minimisation functional:

$$\frac{d}{dx} \int_\Gamma \left[\int_0^T \frac{m_e}{\rho} \frac{cos(\alpha(x,t))}{\pi\, h(x,t)^2} cos(\gamma(x,t))^n \left(\frac{n+1}{2}\right) dt \right] d\Gamma = 0 \quad (29)$$

Since the coating thickness cannot be equal to 0, a constraint must be introduced using a penalty function [7].

Considering d as the thickness of the coating, to equalise the thickness across the substrate surface, the following constraint is introduced:

$$d(x) = C \quad (30)$$

where C is the thickness to be obtained at the end of the coating process.

A penalty function $\phi(\lambda, y)$ for $\lambda \geq 0, y \in \mathbb{R}$, is now introduced which satisfies the following conditions:

- ϕ is continuous.
- $\phi(\lambda, y) \geq 0$ for all λ and y.
- $\phi(\lambda, y) = 0$ for $y \leq 0$ and ϕ is strictly increasing for both $\lambda > 0$ and $y > 0$.

The penalty function is defined as follow.

$$\phi(\lambda, y) = \begin{cases} 0, & d(x) - C = Y(x) = 0 \\ \lambda Y(x)^n, & Y(x) \neq 0 \end{cases} \quad (31)$$

where λ is the penalty parameter. The accuracy of the optimisation model increases with increasing value of λ; to obtain a reasonable estimate of the minimiser this process should be repeated.

The penalty function is now introduced into Equation 28, and the entire expression will be minimised taking into account the constraint (which is the required coating thickness), giving an equation of the form:

$$\widetilde{D_S} = D_S(x, y) + \phi(\lambda, y) \quad (32)$$

Finally, the minimisation functional (Equation 32) can be written as:

$$\widetilde{D_S} = \frac{d}{dx}\left(\int_{\Gamma} \left[\int_0^T \frac{m_e}{\rho} \frac{cos(\alpha(x,t))}{\pi\, h(x,t)^2} cos(\gamma(x,t))^n \left(\frac{n+1}{2}\right) dt \right] d\Gamma + \phi(\lambda, y) \right) = 0 \quad (33)$$

3.5 Conclusion:

In this Chapter, first of all, a mathematical model based on current literature has been presented and demonstrated (Equation 17), also known as Knudsen's Law of Emission. It has been shown that, in order to predict the coating thickness and obtain an accurate distribution (matching experimental evidence), the calculation of all the unknown parameters of the equation is necessary. All the geometrical parameters, such as the angles and the distances between the source and the points of interest can be calculated using a simple computer aided design model. The only unknown remaining is the parameter n, and by using the equation presented earlier as well as exploiting experimental results, this parameter can be determined.

It is therefore possible to predict the coating thickness on a rotating substrate with an arbitrary shape.

Finally, a numerical optimisation model using a penalty method was presented in order to optimise the coating thickness and obtain a homogenised thickness distribution across the surface of a rotating substrate of arbitrary shape. Solving this model requires a complex numerical (finite element) approach, and will not be carried out within the present study, but will be the aim of future studies in this field.

4. Static Model

In this Chapter, the main objective is to solve the parameter n which depends on the rate of evaporation. This parameter will be determined using experimental results, and will then be used to calculate and predict the coating thickness for different cases of inclined and rotating substrates.

4.1 Experimental Results

In order to solve the parameter n, experimental coating distribution tests were conducted using an EB-PVD smart coater (see Figure 3). The tests involve the coating of a

410×150mm wire mesh made of AISI314 stainless steel (see Figure 21) using a ceramic ingot. The mesh is composed of 6×16 elements and 7×17 nodes representing the points of interest across the meshed substrate. The mesh sample was sandblasted and cleaned, and then placed horizontally in the smart coater at 365mm above the source for 1200s coating time (see Table 3 for coating parameters).

Figure 21: Wire mesh used for the distribution test (Photographed by M. Du Plessis, 2014).

Table 3: Parameters for EB-PVD coating process on a wire mesh sample.

Coating time	1200s
Coating mean temperature	978ºc
O_2/Argon flow ratio	90/10
Coating chamber pressure	0.01251 mbar
Emission Current	2.77A
Ingot feed rate	1.6mm/min
Ingot used	32.01mm
Ingot dimension (⌀)	D=50mm
Mesh weight gain	17.75g
Substrate dimensions	410×150mm
Elements size	25×25mm
Wire diameter	3mm
Material	AISI314

After the coating process was completed, the coating thickness was measured at each node of the wire mesh (see Table 4). The thickness distribution was then represented graphically as shown in Figure 22.

Table 4: Coating thickness measured in each node of the wire mesh (µm).

	Y position																
X position	1	1	2	3	4	5	6	7	8	9	10	11	12	13	14	15	16	17
	2	159	173	206	223	257	288	307	319	327	324	312	295	275	250	215	204	198
	3	152	182	207	234	260	291	318	333	344	341	323	309	283	249	223	213	199
	4	164	177	207	240	266	287	318	333	343	334	330	307	288	265	227	216	194
	5	170	176	202	232	261	288	308	320	350	342	316	295	274	245	216	204	198
	6	166	175	190	215	245	277	288	306	324	313	308	283	261	233	206	175	172
	1	143	171	192	202	229	251	273	285	290	298	270	250	230	205	202	170	173

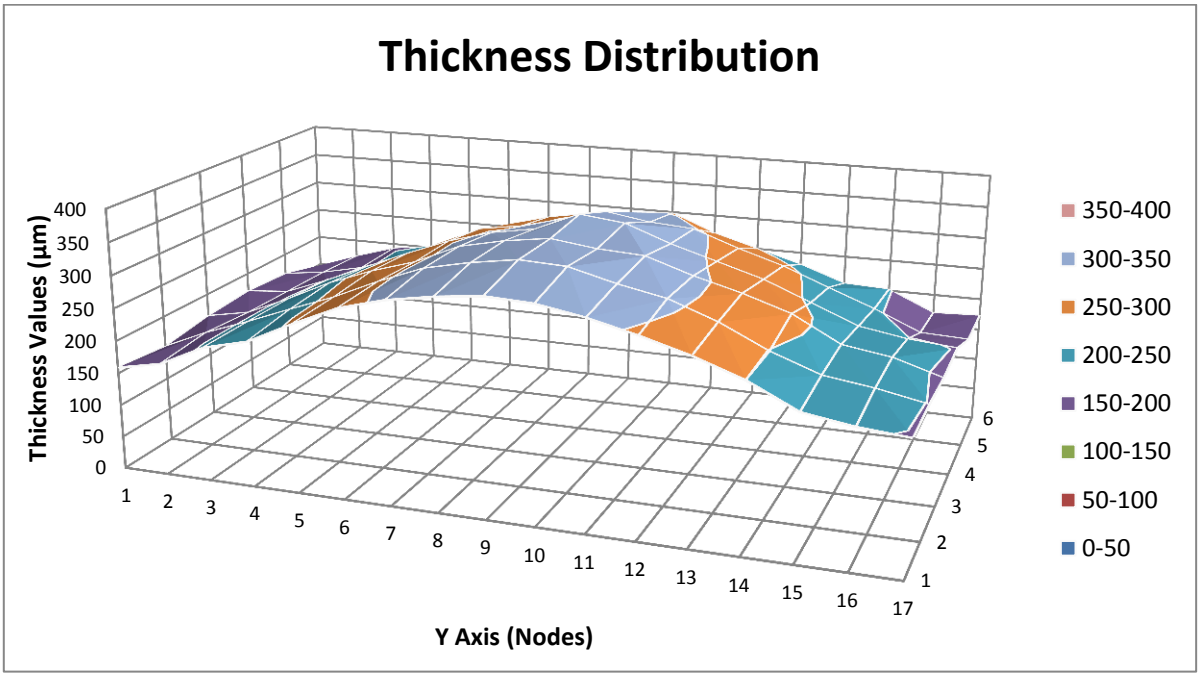

Figure 22: Thickness distribution of a coated wire mesh (µm).

According to the results, it is clearly shown that the distribution is not equally spread across the substrate surface. The maximum thickness of 350µm is located at the centre point of the working area exactly above the vapor source while the minimum thickness of 143µm is located at the extreme side of the mesh; this result is expected since the thickness is highly affected by the distance that separates the source from the point of interest as well as the angles of incidence. It is also noticeable that the thickness distribution is bell-shaped; thus, the coating thickness distribution can be considered as two times symmetric with respect to the two axes X and Y.

This experiment provides valuable information which will allow the calculation of the parameter n, such as the thickness in each point of the mesh, the ingot feed rate (1.6mm/min) and the total ingot used during the coating period of 1200s (32.01mm).

Knowing the shape and the dimensions of the ingot, the total volume evaporated (V_e) during the coating process can be calculated as follow:

$$S_I = \pi \times R_I^2 = \pi \times 25 = 1963.5\, mm^2 \quad (34)$$

$$V_e = S_I \times H_{used} = 1963.5 \times 32.01 = 62851.488\, mm^3 \quad (35)$$

4.2 Numerical Model

In this part of the chapter, a numerical model has been established using a computer aided design software (see Figure 23). This model is an exact replica of the wire mesh used earlier for the experimental work. Thus, using the software, the geometrical angles and the distances between the points of interest and the vapor source can be determined. This will allow the resolution of the parameter n using Equation 17 established in the previous chapter.

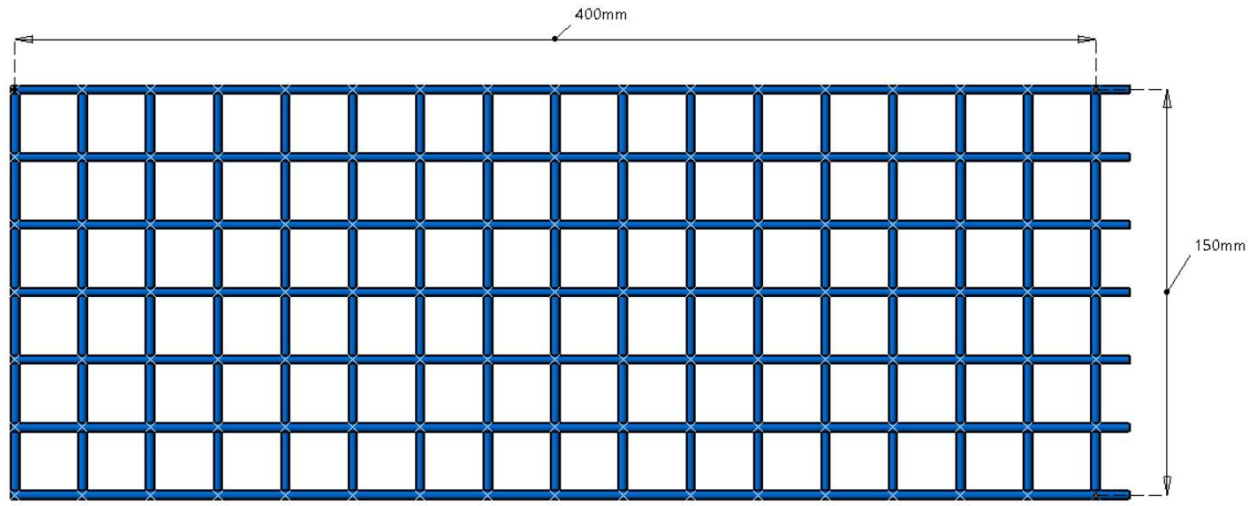

Figure 23: Numerical model of the wire mesh sample.

Since the substrate is positioned horizontally above the vapor source, the angles γ and α are equal (see Figure 24). Thus, the thickness equation becomes:

$$d_s = V_e \frac{cos(\alpha)^{n+1}}{\pi\, h^2} \left(\frac{n+1}{2}\right) \quad (36)$$

where V_e is the total volume evaporated.

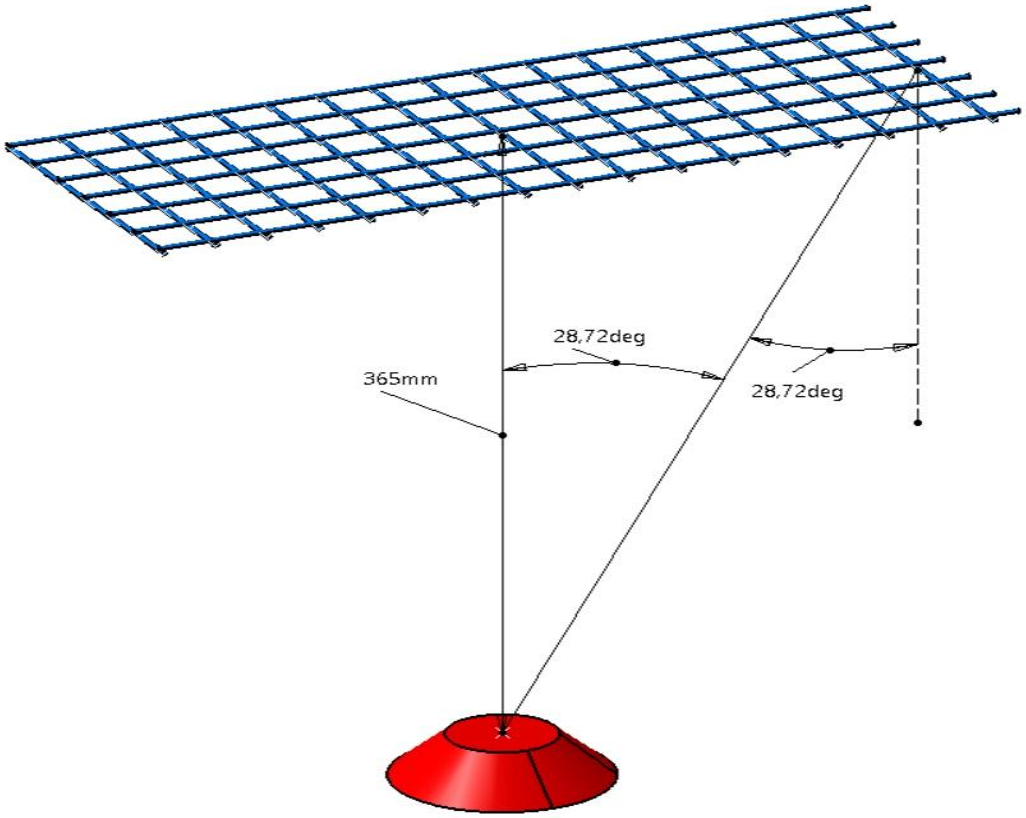

Figure 24: Measurement of the different geometrical angles.

Since this is a symmetric problem, the angles and distances have been determined only for the ¼ of the mesh. The results are presented in the tables below (Table 5 and 6).

Table 5: The angle α measured for each node of the wire mesh (Deg).

	Y position									
X position	**0**	**1**	**2**	**3**	**4**	**5**	**6**	**7**	**8**	**9**
	1	30.336	27.548	24.677	21.771	18.905	16.203	13.872	12.221	11.611
	2	29.458	26.503	23.422	20.246	17.030	13.872	10.964	8.707	7.800
	3	28.908	25.842	22.618	19.252	15.770	12.221	8.707	5.533	3.918
	4	28.720	25.615	22.341	18.905	15.322	11.611	7.800	3.918	0

Table 6: The distance h measured for each node of the wire mesh (mm).

0	**1**	**2**	**3**	**4**	**5**	**6**	**7**	**8**	**9**
1	422.907	411.673	401.684	393.033	385.811	380.099	375.965	373.464	372.626
2	419.196	407.860	397.755	389.037	381.739	375.965	371.786	369.256	368.409
3	416.953	405.555	395.411	386.620	379.276	373.464	369.256	366.708	365.855
4	416.203	404.784	394.620	385.811	378.451	372.626	368.409	365.855	365

Finally, the parameter n can be solved since all the unknowns of the equation have been determined - the distances and the angles (Table 5 and 6) from the numerical model using

the computer aided design software and the coating thickness in each node of the mesh (Table 4) as well as the total volume evaporated V_e during the coating process from the experimental results.

It should be noted that the angles were measured in degree and converted to radian before using them in the equation.

The Equation 37 to be solved is demonstrated below.

$$d_s = V_e \frac{cos(\alpha)^{n+1}}{\pi\, h^2} \left(\frac{n+1}{2}\right)$$

$$\Leftrightarrow \frac{2\times d_s\times\pi\times h^2}{V_e} = cos(\alpha)^{n+1} \times (n+1)$$

$$\Leftrightarrow E = \frac{2\times d_s\times\pi\times h^2}{V_e} - \cos(\alpha)^{n+1} \times (n+1) = 0 \quad (37)$$

where d_s is the thickness measured for each node of the sample, h is the distance separating the source from the point where the thickness was measured and V_e is the total volume evaporated during the 1200s coating process.

To calculate the parameter n, Equation 37 has been solved for each node of the wire mesh, after which the average has been calculated as shown in the following table.

Table 7: The parameter n calculated for each node of the mesh.

0	1	2	3	4	5	6	7	8
1	5.791182	5.125306	4.779072	3.977087	4.064122	4.118591	4.035322	3.986468
2	6.223402	4.697786	4.057614	3.812260	3.669919	3.729946	3.800467	3.798669
3	6.514405	3.852754	3.720690	3.700154	3.555827	3.429330	3.570404	3.573247
4	6.617723	3.676737	3.450202	3.408221	3.378721	3.376214	3.351531	3.325415
5	6.514405	3.742515	3.134388	3.057737	3.127812	3.258268	3.117564	3.195028
6	4.064209	3.899145	3.453736	2.925847	2.989532	2.991584	3.065753	3.072547

9	10	11	12	13	14	15	16	17
4.037198	4.074903	4.131995	4.276711	4.574297	5.033271	5.402836	7.310159	5.791182
3.884278	3.920921	3.883401	4.073919	4.206899	4.273660	4.815417	8.006493	6.223402
3.639715	3.587282	3.752917	3.775768	4.021549	4.404401	4.517795	8.491170	6.514405
3.661422	3.626040	3.469456	3.493461	3.640586	3.742267	3.946544	5.644833	6.617723
3.380042	3.292956	3.418914	3.360734	3.452505	3.514603	3.684179	3.742515	6.514405
3.087165	3.267970	3.017502	2.973561	3.010776	3.004079	3.846775	3.837012	6.223402

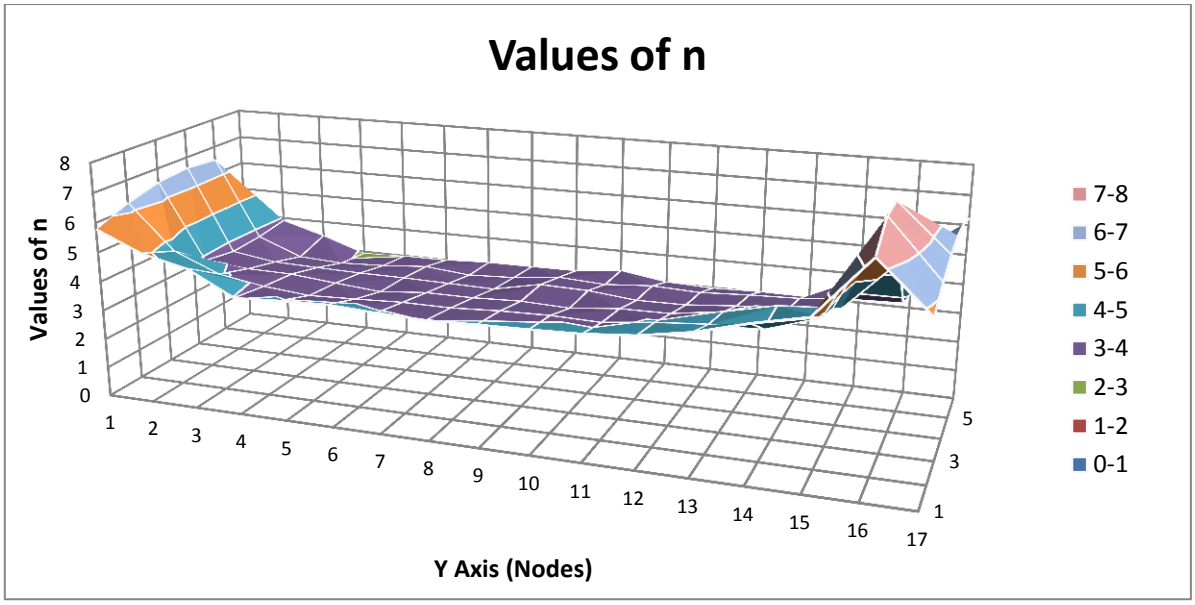

Figure 25: Values of n calculated for each node of the sample.

It is noticeable that the values at the extreme sides of the mesh are very high in comparison with the other values; this result is expected since experimental measurements of thickness values have been used. Those experimental values can be incorrect due to measurement errors at the edges of the substrate.

Based on the results obtained from Table 7 and the graph (Figure 25), the average value of the parameter n can be calculated, giving $n = 4.145845$.

4.3 Effect of the Parameter n on the Thickness Distribution

The parameter n, which is directly dependent on the rate of evaporation, has a very important effect on the coating thickness distribution across the substrate surface.

In this section, the coating thickness of the wire mesh will be calculated for two different values of n. Using the same configuration, i.e. the sample is placed at the same distance from the vapor source (365mm) and in a horizontal position, the coating thickness was calculated for a value of $n = 4$ (see Table 8).

Table 8: Coating thickness for a wire mesh sample with $n = 4$ (mm).

0	1	2	3	4	5	6	7	8	9
1	0.133927	0.161695	0.192036	0.223647	0.254650	0.282683	0.305165	0.319767	0.324835
2	0.142448	0.172577	0.205658	0.240235	0.274288	0.305165	0.330003	0.346162	0.351772
3	0.147896	0.179563	0.214401	0.250943	0.287001	0.319767	0.346162	0.363349	0.369323
4	0.149775	0.181977	0.217426	0.254650	0.291406	0.324835	0.351772	0.369323	0.375422

These results match the experimental results presented earlier (Table 4) which clearly shows that the mathematical model used can predict the coating thickness with enough accuracy (see Figure 26 and 27).

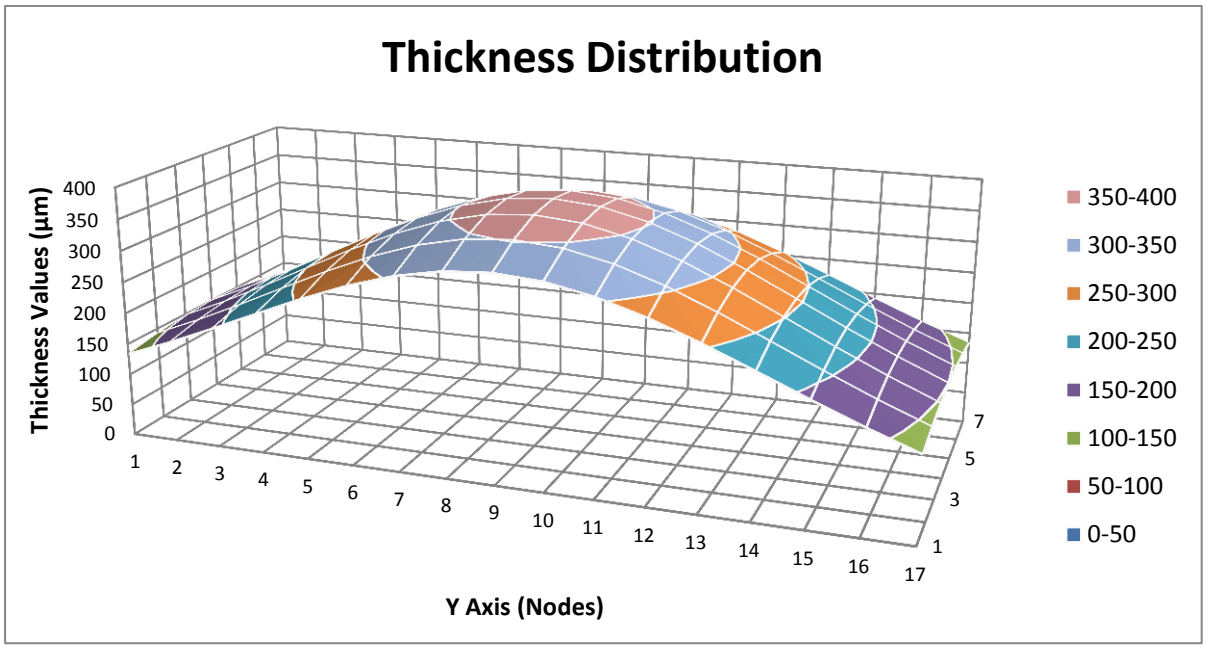

Figure 26: Thickness distribution for a wire mesh with $n = 4$.

A comparison between the two results has been made, the following graphic shows the absolute error ($\delta = experimental\ values - numerical\ values$).

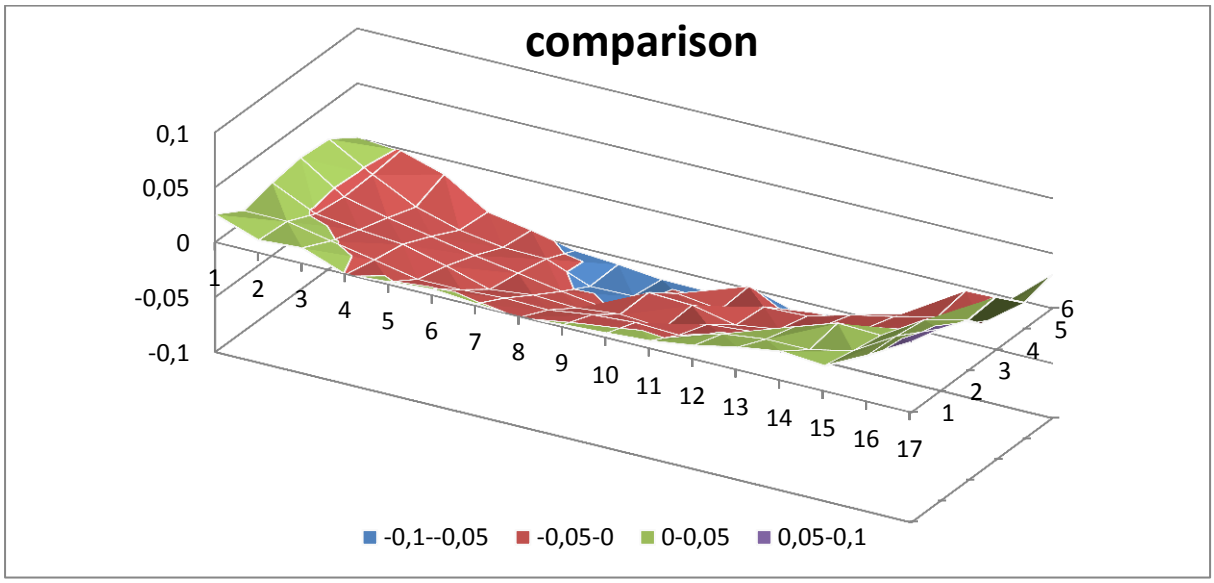

Figure 27: Comparison between the experimental results and the numerical results.

The following table represent the relative error between the two results (%):

$$\delta_r = \frac{\delta}{|experimental\ value|} \tag{38}$$

Table 9: Relative error between the experimental results and the numerical results (%).

0	1	2	3	4	5	6	7	8	9
1	15.769	6.534	6.778	-0.290	0.914	1.846	0.597	-0.240	0.662
2	6.284	5.177	0.648	-2.664	-5.495	-4.867	-3.774	-3.952	-2.259
3	9.819	-1.448	-3.575	-4.559	-7.890	-11.410	-8.850	-9.113	-7.674
4	11.896	-3.395	-7.636	-9.762	-11.640	-12.780	-14.210	-15.410	-7.263
5	10.905	-2.607	-12.840	-16.710	-17.140	-15.430	-20.190	-18.740	-13.980
6	0.386	-0.922	-7.113	-18.920	-19.770	-21.570	-20.880	-21.460	-21.300

0	10	11	12	13	14	15	16	17
1	1.306	2.190	4.175	7.400	10.540	10.680	20.730	32.360
2	-1.513	-2.167	1.240	3.078	3.519	7.776	18.970	28.410
3	-8.787	-4.897	-4.158	0.346	5.304	5.550	16.860	23.760
4	-7.989	-11.320	-10.110	-6.352	-3.938	-0.659	10.790	24.350
5	-16.080	-12.390	-12.990	-9.962	-7.700	-4.078	-2.607	14.010
6	-16.160	-22.220	-22.060	-19.250	-17.180	-1.811	-1.515	17.660

It is clearly noticeable that the maximum error values are located at the edges of the wire mesh; these errors are due to the measurements on the rounded surfaces of the mesh wires not having been ta ken normal to the plume direction.

In order to detect the effect of the parameter n on the coating thickness, another calculation of the thickness has been conducted for the same wire mesh, but with n equal to 1.

Table 10 and the graphic below (Figure 28) show the results obtained.

Table 10: Coating thickness (mm) for a wire mesh with $n = 1$.

0	1	2	3	4	5	6	7	8	9
1	0.083325	0.092798	0.102380	0.111695	0.120296	0.127693	0.133401	0.137012	0.138249
2	0.086315	0.096317	0.106474	0.116356	0.125512	0.133401	0.139501	0.143365	0.144688
3	0.088186	0.098526	0.109032	0.119292	0.128804	0.137012	0.143365	0.147390	0.148770
4	0.088825	0.099280	0.109909	0.120296	0.129931	0.138249	0.144688	0.148770	0.150169

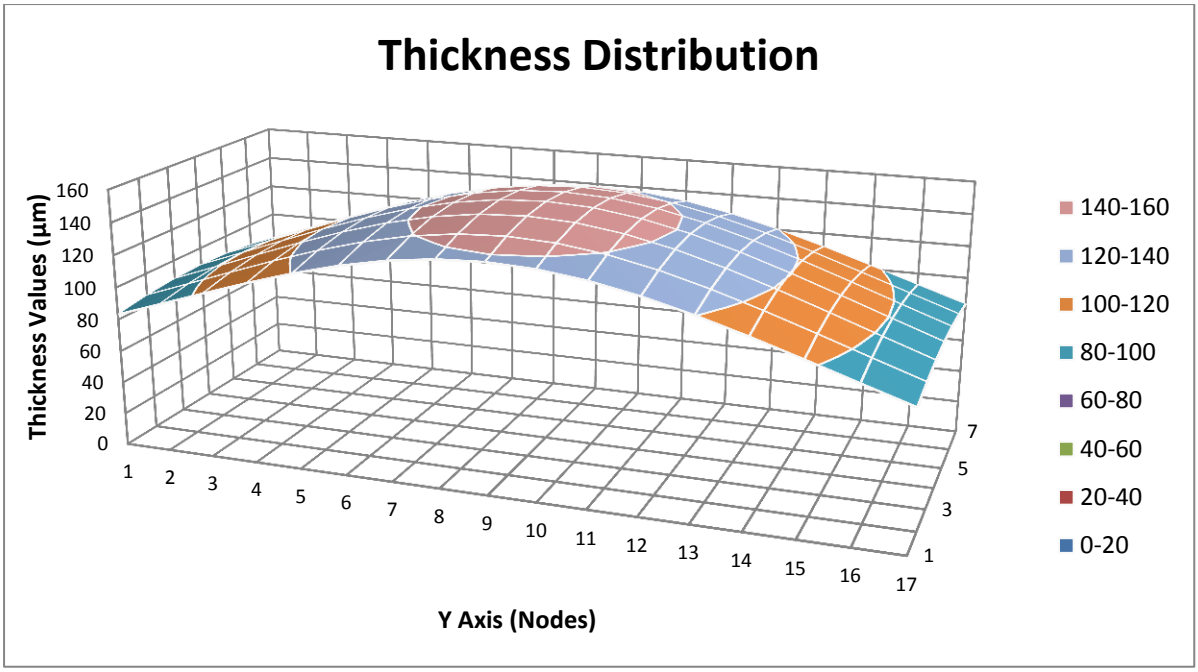

Figure 28: Thickness distribution (µm) for a wire mesh with $n = 1$.

Considering these results (for $n = 1$), it is clear that the parameter n has a very important effect on the coating thickness. The values of the coating thickness clearly decreased in comparison with the results for $n = 4$. This effect and behaviour can be explained by recalling the definition of the parameter n. As already mentioned, n is a parameter depending on the rate of evaporation, which has a direct effect on the shape of the vapor plume (see Figure 12). That is, as the parameter increases, the vapor plume shape changes and the plume becomes more focused, consequently, less ceramic particles are wasted and the substrate surface receives a bigger flow of ceramic particles.

4.4 Inclined Wire Mesh Model

In the previous part of this chapter, the parameter n has been determined. This parameter will allow the prediction of the coating thickness on any substrate in any configuration. In this section, another example will be presented, consisting of the same wire mesh but inclined by 15º with respect to the horizontal plan.

The method used in this calculation consists of:

- The angles α and γ as well as the distances h in this new configuration (15º inclined mesh) will be measured using a computer aided design model.

- All the values of the angles and the distances, the value of the parameter n to be calculated, and the total volume evaporated V_e, will be introduced into the Equation 17 in order to calculate the coating thickness.
- Finally, the thickness distribution results will be presented.

In this case, since the sample is inclined, not only does the problem becomes symmetric only with respect to the Y-axes but also the two angles α and γ are not equal anymore (see Figure 29). Hence, the measurements have been carried out for half the wire mesh and the equation used to predict the thickness is Equation 17 as follows:

$$d_s = \frac{M_e}{\rho}\frac{cos(\alpha)}{\pi\, h^2} cos(\gamma)^n \left(\frac{n+1}{2}\right) \quad (17)$$

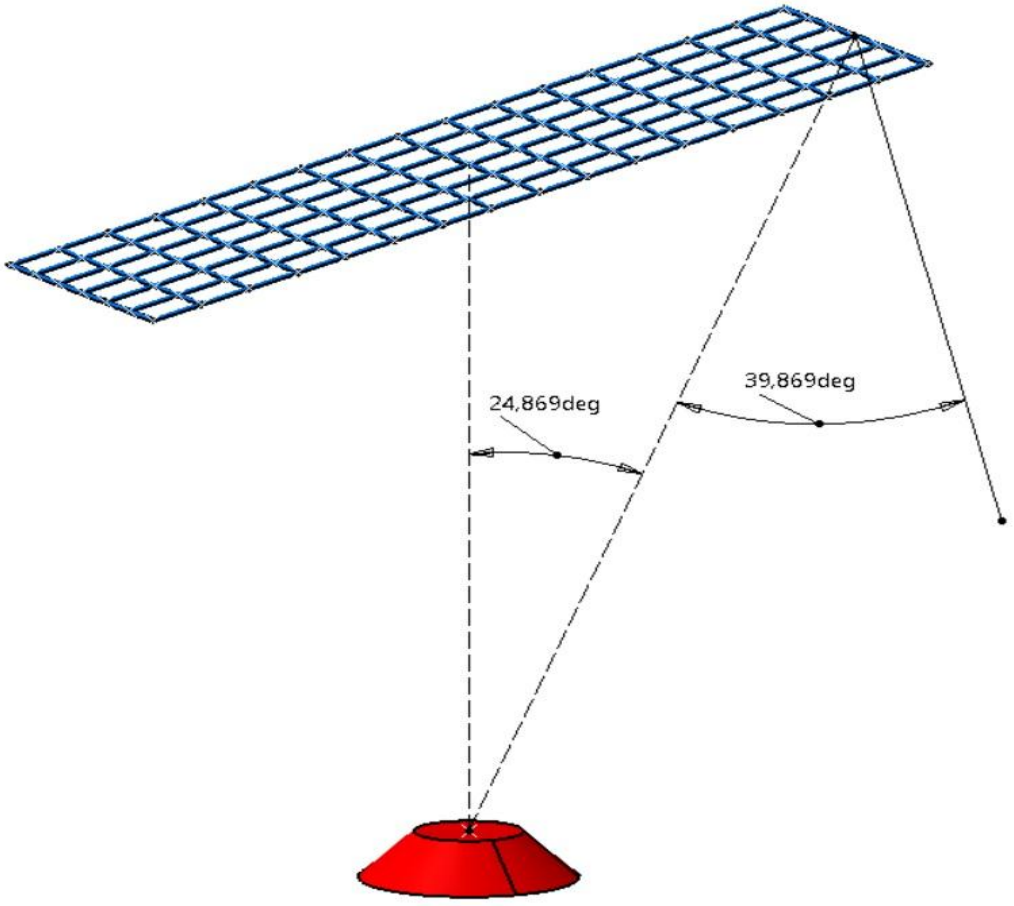

Figure 29: Wire mesh sample inclined by 15º from in respect to the horizontal plan.

The methodology applied in this calculation is explained in Figure 30 below.

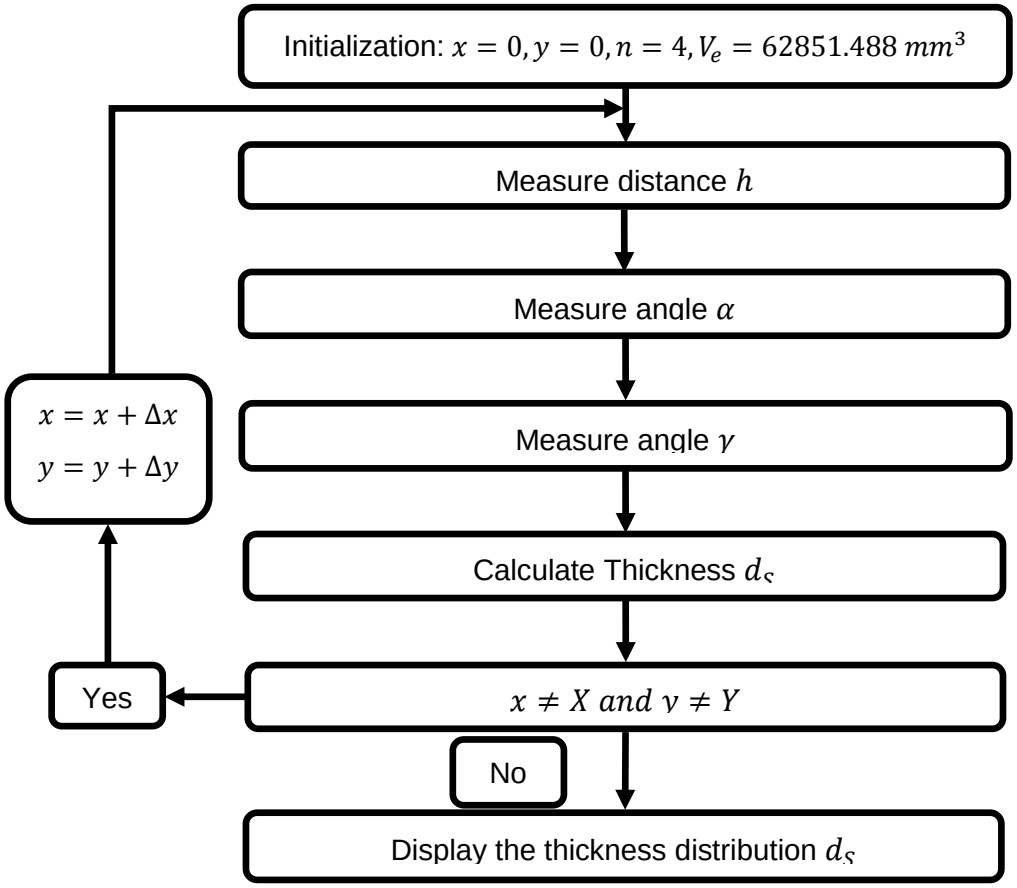

Figure 30: Graph representing the methodology applied to calculate the coating thickness for the inclined wire mesh.

The following tables present the angles and the distance measurements for each node in this new configuration.

Table 11: Angles γ (deg) measured for each node of the inclined mesh.

0	1	2	3	4	5	6	7	8	9	10	11	12	13	14	15	16	17
1	33.488	30.046	26.574	23.137	19.830	16.790	14.218	12.394	11.611	11.975	13.280	15.177	17.373	19.683	21.999	24.262	26.439
2	32.500	28.871	25.169	21.448	17.783	14.290	11.170	8.804	7.800	8.501	10.422	12.897	15.550	18.205	20.785	23.250	25.586
3	31.877	28.123	24.264	20.388	16.395	12.503	8.781	5.537	3.918	5.346	8.188	11.275	14.319	17.240	20.006	22.610	25.051
4	31.664	27.867	23.951	19.949	15.899	11.839	7.811	3.853	0	3.719	7.282	10.673	13.881	16.902	19.738	22.391	24.869
5	31.877	28.123	24.264	20.388	16.395	12.503	8.781	5.537	3.918	5.346	8.188	11.275	14.319	17.240	20.006	22.610	25.051
6	32.500	28.871	25.169	21.448	17.783	14.290	11.170	8.804	7.800	8.501	10.422	12.897	15.550	18.205	20.785	23.250	25.586
7	33.488	30.046	26.574	23.137	19.830	16.790	14.218	12.394	11.611	11.975	13.280	15.177	17.373	19.683	21.999	24.262	26.439

Table 12: Angles α (deg) measured for each node of the inclined mesh.

0	1	2	3	4	5	6	7	8	9	10	11	12	13	14	15	16	17
1	20.164	17.335	14.826	12.935	12.041	12.395	13.891	16.170	18.887	21.806	24.783	27.728	30.591	33.339	35.953	38.427	40.758
2	18.326	15.049	11.967	9.434	8.120	8.653	10.747	13.646	16.865	20.170	23.442	26.618	29.663	32.556	35.289	37.860	40.271
3	17.098	13.451	9.800	6.386	4.154	5.136	8.233	11.827	15.492	19.096	22.580	25.914	29.080	32.068	34.877	37.510	39.971
4	16.664	12.867	8.951	4.949	0.899	3.161	7.189	11.147	15	18.719	22.282	25.673	28.881	31.902	34.738	37.391	39.869
5	17.098	13.451	9.800	6.386	4.154	5.136	8.233	11.827	15.492	19.096	22.580	25.914	29.080	32.068	34.877	37.510	39.971
6	18.326	15.049	11.967	9.434	8.120	8.653	10.747	13.646	16.865	20.170	23.442	26.618	29.663	32.556	35.289	37.860	40.271
7	20.164	17.335	14.826	12.935	12.041	12.395	13.891	16.170	18.887	21.806	24.783	27.728	30.591	33.339	35.953	38.427	40.758

Table 13: Distance h (mm) measured for each node of the inclined mesh.

0	1	2	3	4	5	6	7	8	9	10	11	12	13	14	15	16	17
1	375.583	369.338	364.704	361.743	360.494	360.977	363.185	367.085	372.626	379.735	388.326	398.303	409.565	422.010	435.535	450.043	465.443
2	371.399	365.083	360.395	357.397	356.134	356.623	358.857	362.804	368.409	375.597	384.281	394.361	405.732	418.291	431.933	446.558	462.074
3	368.866	362.506	357.784	354.764	353.491	353.984	356.235	360.210	365.855	373.093	381.834	391.976	403.415	416.044	429.757	444.454	460.041
4	368.018	361.643	356.909	353.882	352.606	353.100	355.356	359.342	365	372.255	381.014	391.178	402.640	415.292	429.029	443.750	459.361
5	368.866	362.506	357.784	354.764	353.491	353.984	356.235	360.210	365.855	373.093	381.834	391.976	403.415	416.044	429.757	444.454	460.041
6	371.399	365.083	360.395	357.397	356.134	356.623	358.857	362.804	368.409	375.597	384.281	394.361	405.732	418.291	431.933	446.558	462.074
7	375.583	369.338	364.704	361.743	360.494	360.977	363.185	367.085	372.626	379.735	388.326	398.303	409.565	422.010	435.535	450.043	465.443

Using the data provided in the previous tables, the coating thickness has been calculated for each node and presented in the table below (Table 14).

Table 14: Thickness distribution measured in each node of the sample.

0	1	2	3	4	5	6	7	8	9	10	11	12	13	14	15	16	17
1	0.1610	0.1965	0.2325	0.2663	0.2947	0.3149	0.3250	0.3243	0.3137	0.2949	0.2701	0.2421	0.2129	0.1844	0.1577	0.1336	0.1124
2	0.1741	0.2131	0.2527	0.2898	0.3209	0.3428	0.3534	0.3521	0.3397	0.3184	0.2907	0.2595	0.2274	0.1962	0.1671	0.1411	0.1182
3	0.1827	0.2239	0.2659	0.3048	0.3381	0.3611	0.3720	0.3702	0.3567	0.3336	0.3040	0.2708	0.2367	0.2037	0.1732	0.1458	0.1219
4	0.1856	0.2277	0.2705	0.3106	0.3441	0.3675	0.3785	0.3766	0.3626	0.3389	0.3086	0.2747	0.2399	0.2063	0.1752	0.1474	0.1232
5	0.1827	0.2239	0.2659	0.3048	0.3381	0.3611	0.3720	0.3702	0.3567	0.3336	0.3040	0.2708	0.2367	0.2037	0.1732	0.1458	0.1219
6	0.1741	0.2131	0.2527	0.2898	0.3209	0.3428	0.3534	0.3521	0.3397	0.3184	0.2907	0.2595	0.2274	0.1962	0.1671	0.1411	0.1182
7	0.1610	0.1965	0.2325	0.2663	0.2947	0.3149	0.3250	0.3243	0.3137	0.2949	0.2701	0.2421	0.2129	0.1844	0.1577	0.1336	0.1124

It is clearly shown that the points of maximum coating thickness are not located in the centre of the mesh, but had shifted to the left side (see Figure 31) due to the inclination of the sample. The distance separating the points of maximum thickness from the vapor source is smaller than the distance separating the centre point located exactly above the source from the ingot; therefore, they receive more ceramic particles than the rest of the nodes.

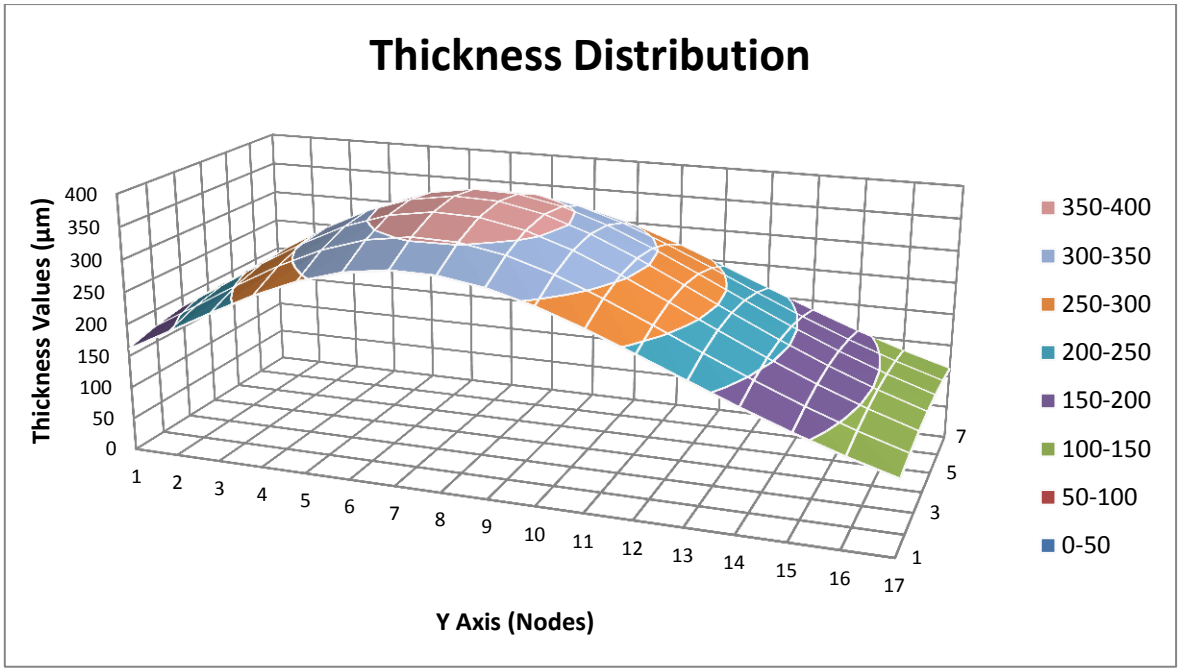

Figure 31: Graph representing the coating thickness distribution for 15º inclined wire mesh.

4.5 Pre-Conclusion

In this chapter, the main objective was to solve the parameter n and then use it to predict the coating thickness on other substrates with different configurations.

Both experimental results as well as a numerical model have been used to determine the unknown parameter n, which was then used later to calculate the coating thickness for a different sample with inclined configuration.

A comparison between experimental results and numerical calculation has been made to verify the accuracy of the mathematical model used to predict the coating thickness.

Regarding the value of the parameter n, coating thickness calculations for a wire mesh sample for two different values of n clearly showed the sensitivity of the coating thickness to this parameter.

Finally, based on the results presented, it can be concluded that the mathematical model used to predict the coating thickness can describe, with sufficient accuracy, the coating distribution across the substrate surface. The objective now is to use the same model to predict the coating thickness on rotating substrates.

5. Coating Thickness Prediction for Rotating Substrates

5.1 Numerical Model and Calculations

In this chapter, the main objective is to predict the coating thickness for a rotating substrate using the same mathematical model presented in the previous chapter.

In order to calculate the thickness, a new sample has been made as shown in the figure below (see Figure 32). This sample is composed of two welded parts - the first part is a cylindrical rod designed to fit in the coater rotating holder, and the second part is a flat surface on which the coating thickness will be calculated.

The surface of the substrate has been meshed with square shaped elements and placed in such a way that the centre of the plate is exactly above the vapor source.

Figure 32: Sample prepared to be coated using the EB-PVD process.

Figure 33 depicts a numerical model of the flat plate rotating sample. As shown, the plate is 30mm × 40mm in dimension with 5×5mm square elements creating 7×9 nodes at which the coating thickness will be calculated. The sample is placed at 365mm from the vapor source which is the distance between the centre of the flat surface and the centre point of the ingot.

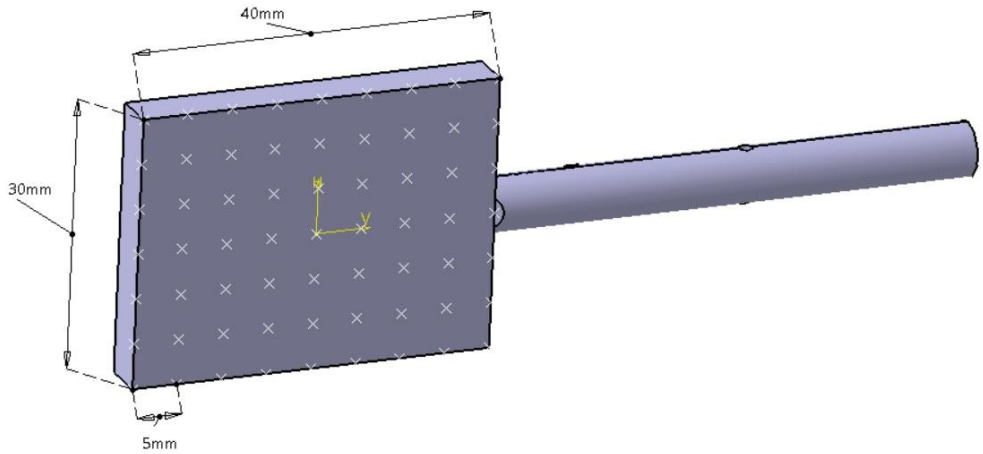

Figure 33: Numerical model for the sample to be coated.

The flat plate is positioned in an initial configuration in such way that the angle β between the flat plate plan and the horizontal plan is equal to 90°. In this calculation, the thickness will be predicted only for the surface of the plate which is opposite to the vapor source. The sample will be rotating 180° ($\beta = 90°\ to\ \beta = -90°$) around the cylindrical part axes.

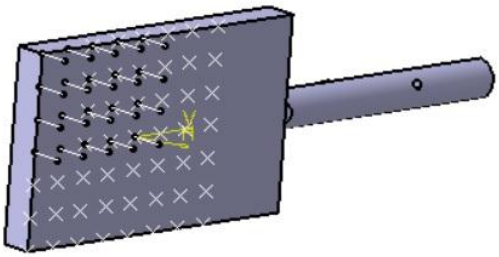

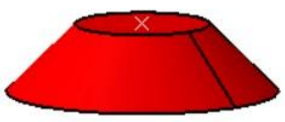

Figure 34: Sample placed above the vapor source with ($\beta = 84°$).

The simulation time is 30 seconds with a time step $\Delta t = 1sec$ and the rotation velocity is $\dot{\beta} = 1rpm = 6^{\circ}/sec$.

This problem is considered as a quasi-steady state problem. This means that the thickness has been calculated for a certain point in each configuration, and the total thickness in that point after the simulation is given by the summation of all the thicknesses calculated during the process. The coating distribution is ultimately given by the representation of the thickness values of all the points of the mesh. Since, the problem is bisymmetric with respect to the X and Y axes, it is enough to calculate the coating thickness values for only ¼ of the flat plate.

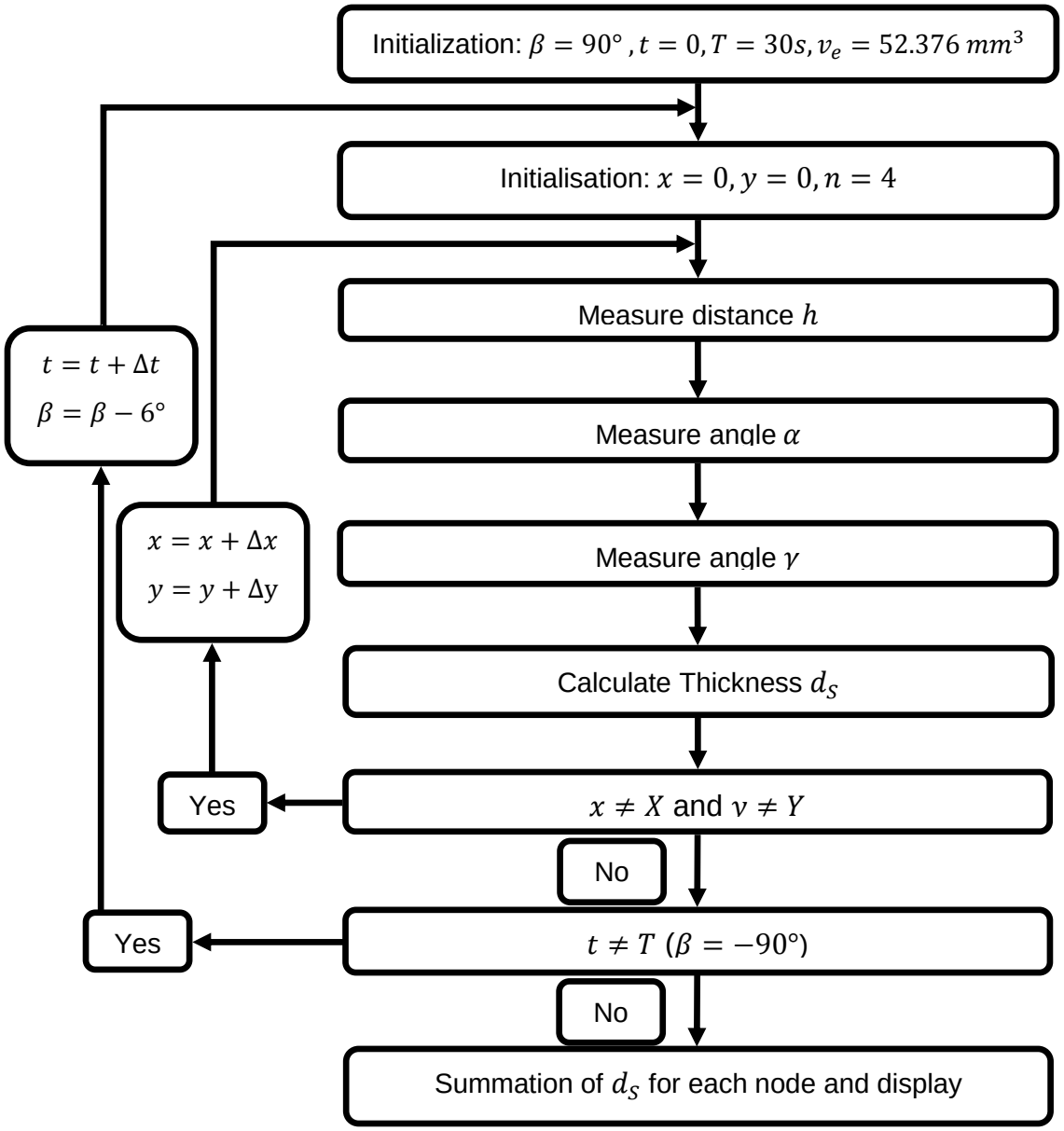

Figure 35: Algorithm representing the methodology applied to calculate the coating thickness for the rotating sample.

Each time step in this calculation is considered as an independent coating thickness calculation problem for a flat plate with a different inclination angle. Thus, the volume evaporated in this case is not the one used in the previous predictions V_e (volume evaporated during 1200sec). Hence, the volume evaporated during one time step (1s) is determined as follows:

$$v_e = \frac{V_e}{1200} = 52.376\ mm^3 \quad (39)$$

In Figure 35, the methodology used in this thickness calculation has been presented with β being the inclination angle between the flat sample and the horizontal plan, T the duration of the simulation and x and y the coordinates of the nodes.

The methodology is similar to the inclined mesh test since this problem has been discretised to become a summation of many iterations. Each iteration has been considered as it was an independent inclined mesh calculation with a different inclination angle.

In order to see the evolution of the iterations, the simulation has been interrupted after 15s, which is the exact time when the flat plate of the substrate is facing the vapor source creating an angle $\beta = 0°$ with the horizontal plan. These results are presented in Table 15 below.

Table 15: Coating thickness calculated (μm) for the flat plate sample after 15s.

0	**1**	**2**	**3**	**4**	**5**	**6**	**7**	**8**	**9**
1	2.9257	2.9387	2.9479	2.9535	2.9554	2.9535	2.9479	2.9387	2.9257
2	2.9870	3.0005	3.0101	3.0158	3.0178	3.0158	3.0101	3.0005	2.9870
3	3.0480	3.0618	3.0717	3.0777	3.0797	3.0777	3.0717	3.0618	3.0480
4	3.1084	3.1227	3.1329	3.1391	3.1411	3.1391	3.1329	3.1227	3.1084
5	3.1681	3.1829	3.1935	3.1999	3.2020	3.1999	3.1935	3.1829	3.1681
6	3.2272	3.2425	3.2534	3.2600	3.2622	3.2600	3.2534	3.2425	3.2272
7	3.2856	3.3013	3.3126	3.3194	3.3216	3.3194	3.3126	3.3013	3.2856

The thickness distribution is presented in Figure 36. As shown, the difference of the thickness values between the upper half of the plate and the bottom one is clear. The coating thickness decreases from the bottom part of the mesh to the upper part and increases from the sides to the centre point, as was expected. Initially, the sample was in a vertical position, and during the rotation of 90°, the upper part of the mesh was kept far from the vapor source in comparison to the bottom part which was very close to the source. Consequently, the bottom part of the substrate surface experienced a greater exposure to the ceramic vapor plume as compared to the upper half.

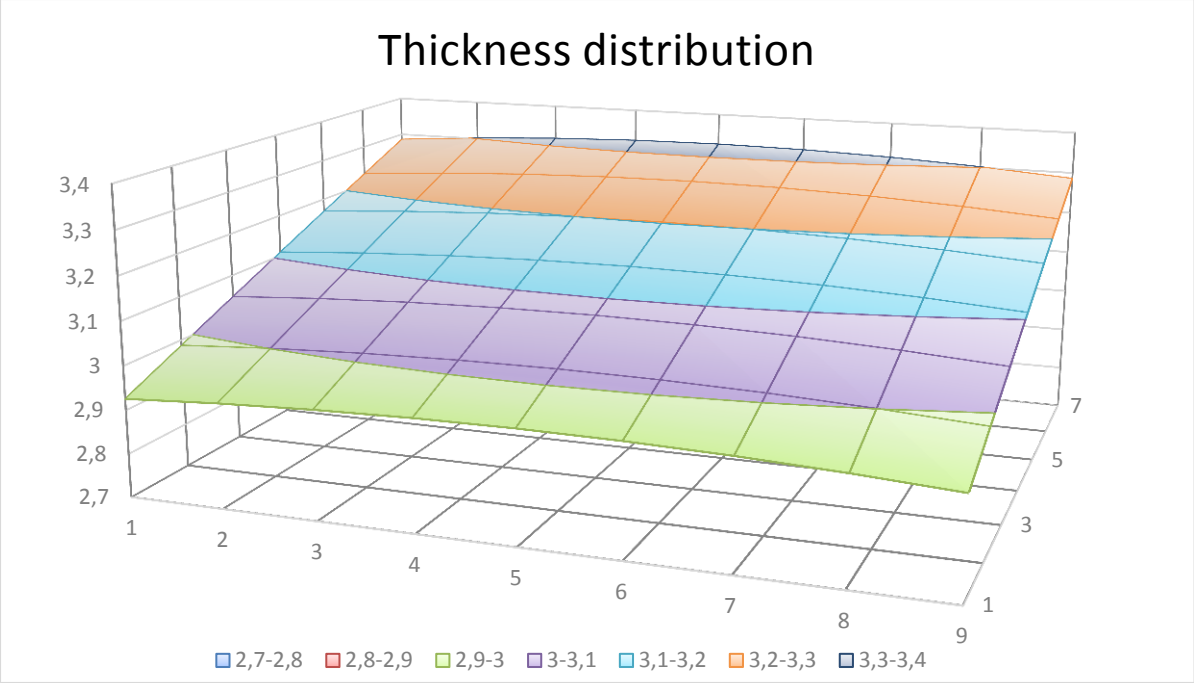

Figure 36: Thickness distribution calculated for the flat plate sample after 15s (µm).

The nodal thickness distribution after 30s of coating time is presented in the table below.

Table 16: Coating thickness values for the flat plate substrate after 30s simulation.

0	1	2	3	4	5	6	7	8	9
1	5.9036	5.9308	5.9503	5.9621	5.9661	5.9621	5.9503	5.9308	5.9036
2	5.9055	5.9328	5.9523	5.9641	5.9680	5.9641	5.9523	5.9328	5.9055
3	5.9068	5.9339	5.9535	5.9652	5.9691	5.9652	5.9535	5.9339	5.9068
4	5.9072	5.9343	5.9538	5.9656	5.9695	5.9656	5.9538	5.9343	5.9072
5	5.9068	5.9339	5.9535	5.9652	5.9691	5.9652	5.9535	5.9339	5.9068
6	5.9055	5.9328	5.9523	5.9641	5.9680	5.9641	5.9523	5.9328	5.9055
7	5.9036	5.9308	5.9503	5.9621	5.9661	5.9621	5.9503	5.9308	5.9036

According to these results, it is noticeable that the variation of the thickness is not very pronounced. This is due to the short coating time and the small dimensions of the sample in comparison with the distance separating the substrate surface from the vapor source.

Nevertheless, the thickness distribution represented in the Figure 37 shows clearly the variation of the thickness values across the surface. Such thickness variations can cause early degradation of the part, especially if this latter is exposed to hostile environmental conditions. For instance, turbine blades are exposed to a very high temperature. The difference of the coating thickness between two different points of the blade surface will certainly has an impact on the heat conductivity in those points (two different conductivity coefficients). Consequently, it will create a temperature gradient inside the part leading to internal constraints that can damage the blade.

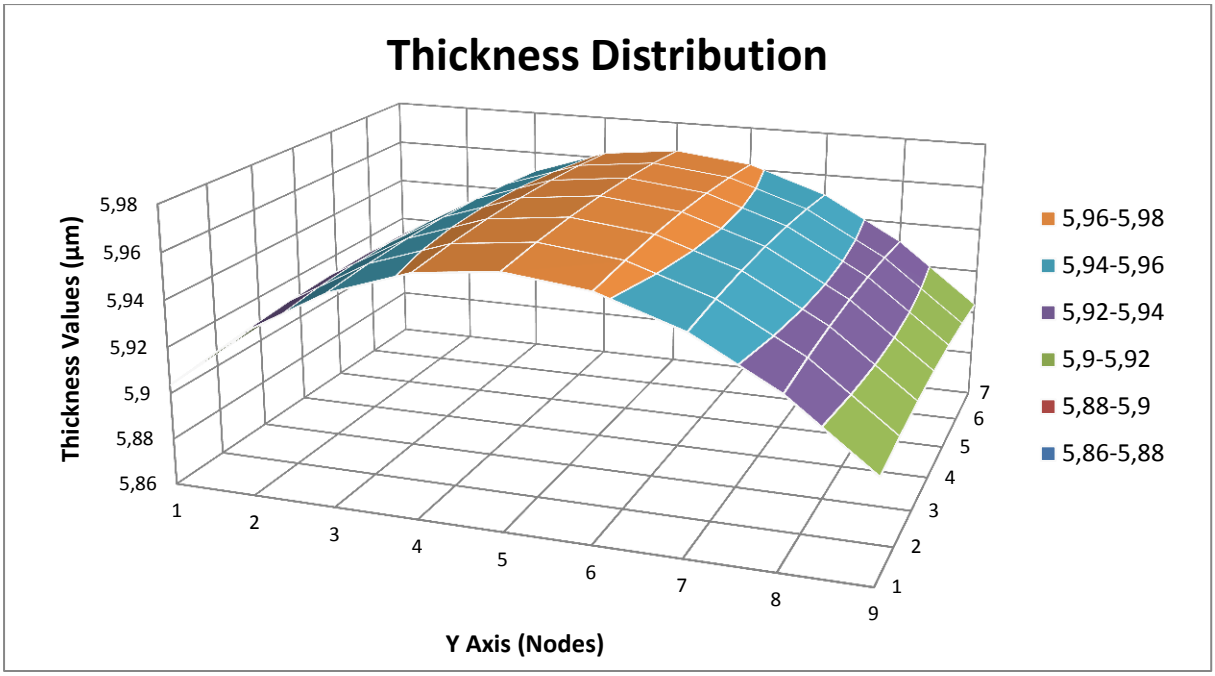

Figure 37: Thickness distribution on the surface of the substrate after 30s simulation.

6. Conclusions

In this research, the main objective was to develop a method to predict the coating thickness. This method was based on developing a mathematical model based on the Knudsen's law of emission capable of predicting the coating thickness values and distribution for arbitrarily shaped rotating parts coated using vapor deposition techniques such as EB-PVD.

The equation used is a function of the total ceramic volume evaporated V_e as well as geometrical parameters that locate the point of interest with respect to the vapor source. Those parameters are:

- The distance h separating the centre of the ingot from the elementary area where the thickness was calculated.
- The angles α and γ (see figure below).
- The rate of evaporation parameter n.

This same model was used to develop a minimisation functional for the optimisation of the thickness distribution, using an optimisation method incorporating a penalty function to set the desired coating thickness. This optimisation model will allow the calculation of the variable speed of rotation through a single revolution which will result in a regular distribution of the ceramic particles across the substrate surface to be obtained.

According to the model, the coating thickness is tightly linked to the geometrical position of the substrate, i.e. the distance between the surface and the vapor source, the inclination angle of the surface and the angle of incidence (which is the angle between the vector generated by the source and the point of interest and the normal vector to the surface at that point).

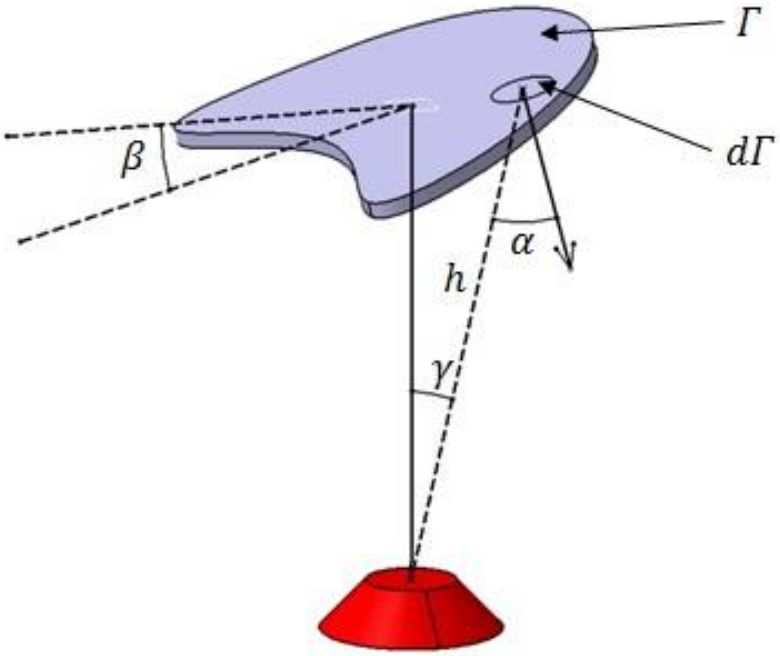

Figure 38 (recalled): Configuration of an arbitrarily-shaped substrate.

In order to calculate the coating thickness, many parameters needed to be determined. Some of these, such as distances and angles, were measured using a computer aided design-model and others were determined by calculation, such as the total ceramic volume evaporated and the parameter n (which is dependent on the rate of evaporation). The amount of ceramic material evaporated was calculated using the geometry of the ingot and the ingot feed rate.

In order to calculate n, experimental values of coating thickness were necessary; therefore, experimental coating tests were conducted for a wire mesh sample. After measuring the thickness throughout the substrate surface, the results were used to determine the rate of evaporation parameter (n).

In this particular area, a model could be developed in order to find a relation between n and the emission current. With such a model at hand, and using the coating machine settings, the parameter n can then be determined without the need for experimental tests.

In this research, the value of n was considered constant because of the short coating time. However, in reality, this parameter can change with respect to time depending on the ingot surface change due to the evaporation, resulting in a concave surface of the ingot.

In Chapter 4, after determining the value of the parameter n (that is, $n = 4$), two sets of calculations were conducted for two different values of n ($n = 4$ and $n = 1$) in order to show clearly the effect of this parameter on the thickness. This test confirmed the expected results: as n increased, the vapor plume became denser and, consequently, less ceramic particles were wasted during the coating process; thus, there was a higher probability that these particles collided with the surface of the substrate.

The inclination of the substrate with respect to the horizontal plan is another important parameter. In order to see how this angle affects the thickness distribution, a coating test was conducted. The sample (wire mesh) was inclined at 15° to the horizontal plan. The results showed that the inclination of the substrate can affect the thickness distribution, but this effect is less pronounced on the thickness values.

According to the experimental results and the comparison with the analytical predictions, this mathematical model can predict with sufficient accuracy the coating distribution and thickness values for static substrates. This model does not take into account the shape of the substrate and works perfectly with any shape, since it calculates the thickness at each point based on its geometrical position with respect to the vapor source.

In the second part of this research, the model was used to calculate the thickness for rotating substrates. For this purpose, another numerical model was created and meshed. This problem was treated as a quasi-steady problem. The substrate was placed at 365mm above the vapor source in a vertical position, which was set as the initial position for the coating simulation. The part was rotated through 180° ($\beta = 90^\circ \ to \ \beta = -90^\circ$) with a rotating velocity $\dot{\beta} = 1\, rpm$, which is equivalent to 6°/s. To solve this problem, each time step was considered as an independent case of an inclined flat plate exposed to the vapor plume for a 1s time step. Then, after 30s simulation time, the summation of the thicknesses for each time step resulted in the total coating thickness.

The results showed that, for this particular coating prediction test, the mathematical model is capable of predicting the thickness distribution for a rotating substrate, since the results obtained matched perfectly the physical predictions. However, an experimental validation needs to be carried out to finally validate the model for rotating surfaces.

In spite of the good results obtained in this research, some problems were observed and need to be investigated. This includes the problem of determining the optimal distance separating the vapor source from the substrate in order to obtain the best vapor distribution across the surface. In this project, the distance was chosen arbitrarily as 365mm.

The second problem observed was the coating accuracy on the edges of the flat plate substrates. Based on the observations in the comparison between experimental and analytical results, there were large differences in the values at the points located on the extreme sides of the sample. The experimental values were higher than the analytically obtained values; hence, further investigations should be carried out to overcome this problem in order to obtain a more accurate prediction of the coating thickness.

7. References

1. J. Singh, J.T. Schriempf, D.E. Wolfe. (1997). **Electron Beam Physical Vapour Deposition Technology: Present and Future Applications.** Technical report, Applied Research Laboratory, PENNSTATE (1–4).
2. E. Lugscheider, C. Barimani, G. Dopper. (1998). **Ceramic thermal barrier coatings deposited with the EB-PVD**. Surface and coatings Technology 98 (1221–1227).
3. J. R. Nicholls, V. Pereira, K. J. Lawsonx and D. S. Rickerby. (May 1998). **Process Control of Deposition Profiles in the Manufacture of EB-PVD Thermal Barrier Coatings.** Paper presented at the RTO AVT Workshop on “Intelligent Processing of High Performance Materials”, held in Brussels, Belgium (13-14), and published in RTO MP-9.
4. I. Fuke, V. Prabhu, S. Baek. (2005). **Computational Model for Predicting Coating Thickness in Electron Beam Physical Vapour Deposition.** Journal of Manufacturing Processes 7 (140–152).
5. J.S. Bernier, W.C.S. Weir, M. Fontecchio, R.D. Sisson, S. Bose. (2002). **Deposition rates of EB-PVD TBCs on cylindrical surfaces**. 26th annual conference on composites, advanced ceramics, materials, and structures, Cocoa Beach FL, United States 23 (854–884).
6. S. Baek, V. Prabhu. (2009). **Simulation model for an EB-PVD coating structure using the level set method**. Journal of Manufacturing Processes 11 (1–7).
7. Kurt Bryan and Yosi Shibberu. **Penalty Functions and Constrained Optimization**. Dept. of Mathematics, Rose-Hulman Institute of Technology (1- 6)

Annexure 1: Equipment Used for Preparing the Sample and the Coating Process

Figure 39: Sand-Blasting machine.

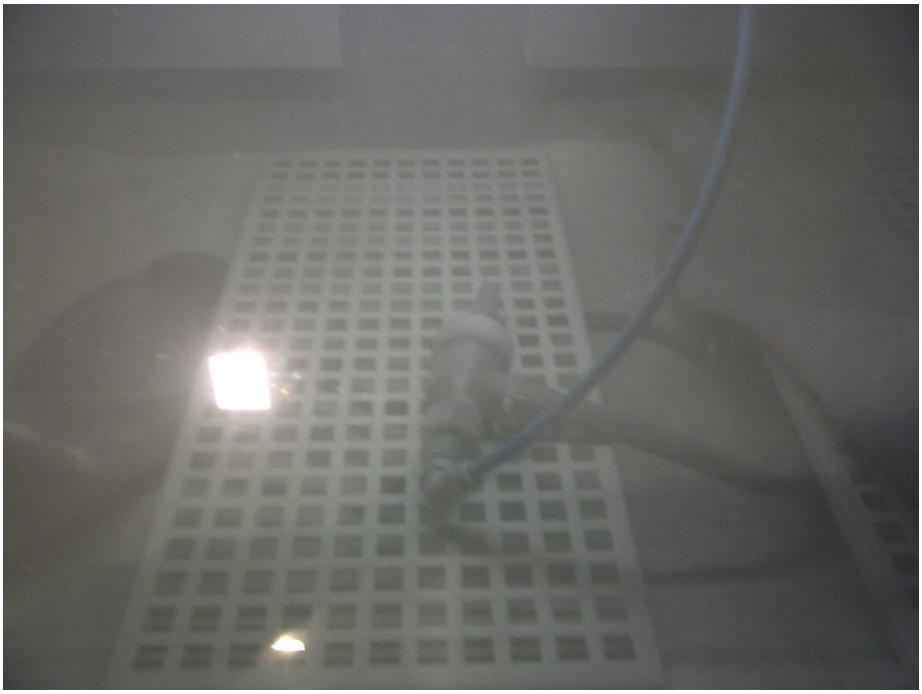

Figure 40: Sand-Blasting machine (inside view).

Figure 41: Flat plate sample before and after sand-blasting.

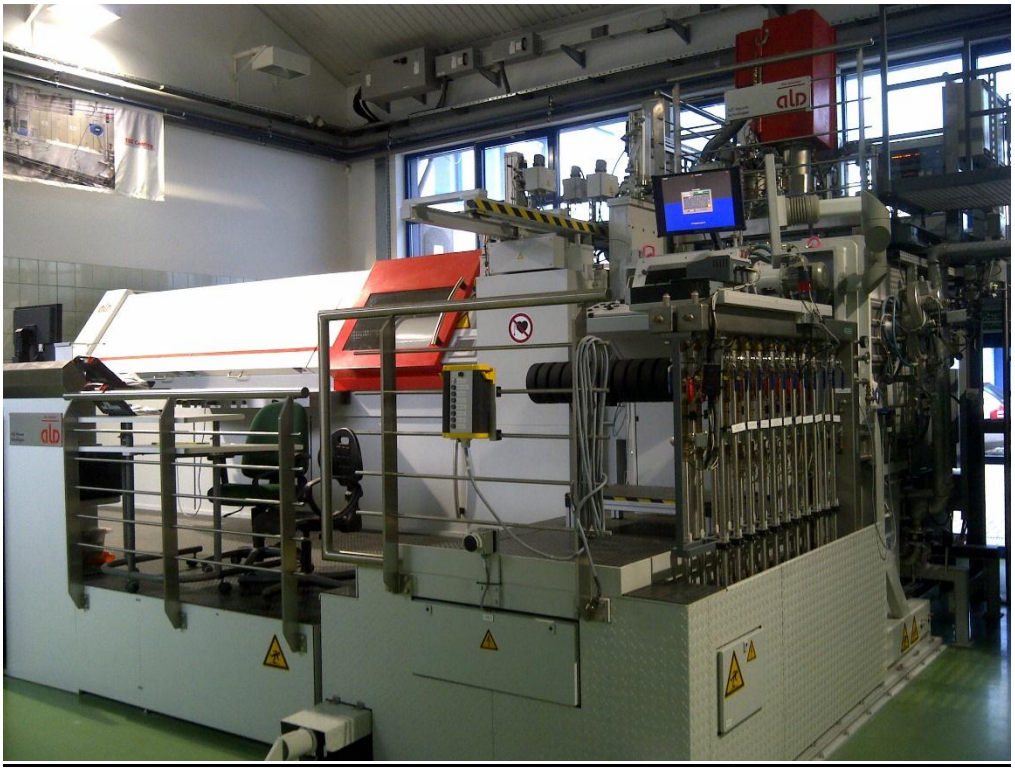

Figure 42: EB-PVD Smart coating machine.

Annexure 2: Coating Thickness Calculation Data

In this annexure, all the measurements and data for every step of the coating thickness calculation of the rotating flat plate sample have been presented.

Step 2: $\beta = 84°$

Table 17: Nodes angles γ (deg).

0	1	2	3	4	5
1	3.023	2.273	1.526	0.790	0.236
2	3.057	2.296	1.536	0.781	0.160
3	3.095	2.323	1.550	0.778	0.081
4	3.136	2.353	1.569	0.785	0

Table 18: Nodes angles α (deg).

0	1	2	3	4	5
1	84.244	84.241	84.238	84.237	84.236
2	84.168	84.164	84.162	84.160	84.160
3	84.090	84.086	84.083	84.081	84.081
4	84.009	84.005	84.002	84.001	84

Table 19: Nodes distances h (mm).

0	1	2	3	4	5
1	380.447	380.217	380.053	379.954	379.921
2	375.480	375.247	375.080	374.980	374.947
3	370.513	370.277	370.108	370.007	369.973
4	365.548	365.308	365.137	365.034	365

Table 20: Thickness d (mm).

0	1	2	3	4	5
1	2.87E-05	2.88E-05	2.89E-05	2.90E-05	2.90E-05
2	2.99E-05	3E-05	3.01E-05	3.01E-05	3.02E-05
3	3.11E-05	3.12E-05	3.13E-05	3.14E-05	3.14E-05
4	3.24E-05	3.25E-05	3.26E-05	3.27E-05	3.27E-05

Step 3: $\beta = 78°$

Table 21: Nodes angles γ (deg).

0	1	2	3	4	5
1	3.052	2.311	1.580	0.889	0.471
2	3.071	2.314	1.561	0.828	0.318
3	3.099	2.328	1.557	0.791	0.161
4	3.136	2.353	1.569	0.785	0

Table 22: Nodes angles α (deg).

0	1	2	3	4	5
1	78.487	78.480	78.475	78.472	78.471
2	78.355	78.327	78.322	78.319	78.318
3	78.179	78.171	78.165	78.162	78.161
4	78.018	78.010	78.005	78.001	78

Table 23: Nodes distances h (mm).

0	1	2	3	4	5
1	380.211	379.981	379.817	379.718	379.685
2	375.320	375.087	374.921	374.821	374.787
3	370.433	370.196	370.027	369.926	369.892
4	365.548	365.308	365.137	365.034	365

Table 24: Thickness d (mm).

0	1	2	3	4	5
1	5.72E-05	5.75E-05	5.76E-05	5.77E-05	5.78E-05
2	5.94E-05	5.97E-05	5.99E-05	6E-05	6.01E-05
3	6.19E-05	6.21E-05	6.23E-05	6.25E-05	6.25E-05
4	6.44E-05	6.47E-05	6.49E-05	6.50E-05	6.50E-05

Step 4: $\beta = 72°$

Table 25: Nodes angles γ (deg).

0	1	2	3	4	5
1	3.098	2.370	1.665	1.030	0.700
2	3.093	2.342	1.601	0.899	0.473
3	3.105	2.335	1.568	0.811	0.239
4	3.136	2.353	1.569	0.785	0

Table 26: Nodes angles α (deg).

0	1	2	3	4	5
1	72.725	72.714	72.706	72.702	72.700
2	72.498	72.487	72.479	72.474	72.473
3	72.266	72.255	72.246	72.241	72.239
4	72.028	72.016	72.007	72.002	72

Table 27: Nodes distances h (mm).

0	1	2	3	4	5
1	379.821	379.591	379.426	379.327	379.294
2	375.057	374.824	374.657	374.557	374.523
3	370.299	370.063	369.894	369.792	369.759
4	365.548	365.308	365.137	365.034	365

Table 28: Thickness d (mm).

0	1	2	3	4	5
1	8.53E-05	8.57E-05	8.592E-05	8.61E-05	8.61E-05
2	8.86E-05	8.90E-05	8.925E-05	8.94E-05	8.95E-05
3	9.20E-05	9.25E-05	9.275E-05	9.29E-05	9.30E-05
4	9.57E-05	9.61E-05	9.642E-05	9.66E-05	9.67E-05

Step 5: $\beta = 66°$

Table 29: Nodes angles γ (deg).

0	1	2	3	4	5
1	3.160	2.448	1.772	1.193	0.923
2	3.122	2.379	1.653	0.987	0.623
3	3.114	2.345	1.582	0.837	0.315
4	3.136	2.353	1.569	0.785	0

Table 30: Nodes angles α (deg).

0	1	2	3	4	5
1	66.957	66.942	66.931	66.925	66.923
2	66.658	66.643	66.632	66.625	66.623
3	66.352	66.336	66.324	66.318	66.315
4	66.038	66.022	66.010	66.002	66

Table 31: Nodes distances h (mm).

0	1	2	3	4	5
1	379.280	379.049	378.884	378.785	378.752
2	374.692	374.458	374.291	374.191	374.158
3	370.114	369.878	369.709	369.607	369.573
4	365.548	365.308	365.137	365.034	365

Table 32: Thickness d (mm).

0	1	2	3	4	5
1	0.000113	0.000113	0.000114	0.000114	0.000114
2	0.000117	0.000117	0.000118	0.000118	0.000118
3	0.000121	0.000122	0.000122	0.000122	0.000123
4	0.000126	0.000126	0.000127	0.000127	0.000127

Step 6: $\beta = 60°$

Table 33: Nodes angles γ (deg).

0	1	2	3	4	5
1	3.234	2.540	1.894	1.366	1.137
2	3.158	2.423	1.714	1.084	0.767
3	3.124	2.358	1.599	0.867	0.388
4	3.136	2.353	1.569	0.785	0

Table 34: Nodes angles α (deg).

0	1	2	3	4	5
1	61.181	61.162	61.148	61.139	61.137
2	60.812	60.792	60.778	60.770	60.767
3	60.435	60.415	60.400	60.391	60.388
4	60.050	60.028	60.012	60.003	60

Table 35: Nodes distances h (mm).

0	1	2	3	4	5
1	378.593	378.362	378.197	378.098	378.065
2	374.229	373.995	373.827	373.727	373.694
3	369.880	369.643	369.474	369.372	369.339
4	365.548	365.308	365.137	365.034	365

Table 36: Thickness d (mm).

0	1	2	3	4	5
1	0.000139	0.000140	0.000140	0.000141	0.000141
2	0.000144	0.000145	0.000145	0.000146	0.000146
3	0.000149	0.000150	0.000151	0.000151	0.000151
4	0.000155	0.000156	0.000156	0.000156	0.000156

Step 7: $\beta = 54°$

Table 37: Nodes angles γ (deg).

0	1	2	3	4	5
1	3.317	2.641	2.025	1.540	1.339
2	3.198	2.473	1.781	1.185	0.903
3	3.135	2.372	1.618	0.900	0.456
4	3.136	2.353	1.569	0.785	0

Table 38: Nodes angles α (deg).

0	1	2	3	4	5
1	55.395	55.371	55.353	55.343	55.339
2	54.960	54.935	54.917	54.906	54.903
3	54.516	54.490	54.471	54.460	54.456
4	54.062	54.035	54.016	54.004	54

Table 39: Nodes distances h (mm).

0	1	2	3	4	5
1	377.768	377.536	377.371	377.271	377.238
2	373.672	373.438	373.270	373.170	373.136
3	369.598	369.361	369.192	369.091	369.057
4	365.548	365.308	365.137	365.034	365

Table 40: Thickness d (mm).

0	1	2	3	4	5
1	0.000165	0.000165	0.000166	0.000166	0.000166
2	0.000170	0.000171	0.000172	0.000172	0.000172
3	0.000176	0.000177	0.000177	0.000178	0.000178
4	0.000182	0.000183	0.000183	0.000184	0.000184

Step 8: $\beta = 48°$

Table 41: Nodes angles γ (deg).

0	1	2	3	4	5
1	3.405	2.747	2.157	1.708	1.528
2	3.241	2.525	1.850	1.285	1.029
3	3.148	2.387	1.638	0.935	0.520
4	3.136	2.353	1.569	0.785	0

Table 42: Nodes angles α (deg).

0	1	2	3	4	5
1	49.597	49.567	49.546	49.533	49.528
2	49.101	49.070	49.047	49.034	49.029
3	48.594	48.562	48.538	48.525	48.520
4	48.077	48.043	48.019	48.005	48

Table 43: Nodes distances h (mm).

0	1	2	3	4	5
1	376.812	376.580	376.414	376.314	376.281
2	373.028	372.793	372.626	372.525	372.492
3	369.273	369.036	368.866	368.765	368.731
4	365.548	365.308	365.137	365.034	365

Table 44: Thickness d (mm).

0	1	2	3	4	5
1	0.000189	0.000190	0.000190	0.000191	0.000191
2	0.000195	0.000196	0.000196	0.000197	0.000197
3	0.000201	0.000202	0.000202	0.000203	0.000203
4	0.000207	0.000208	0.000209	0.000209	0.000209

Step 9: $\beta = 42°$

Table 45: Nodes angles γ (deg).

0	1	2	3	4	5
1	3.494	2.853	2.287	1.866	1.702
2	3.285	2.579	1.920	1.380	1.145
3	3.161	2.402	1.659	0.969	0.578
4	3.136	2.353	1.569	0.785	0

Table 46: Nodes angles α (deg).

0	1	2	3	4	5
1	43.787	43.750	43.724	43.708	43.702
2	43.234	43.195	43.167	43.151	43.145
3	42.670	42.630	42.601	42.584	42.578
4	42.095	42.054	42.024	42.006	42

Table 47: Nodes distances h (mm).

0	1	2	3	4	5
1	375.735	375.502	375.366	375.236	375.203
2	372.303	372.068	371.900	371.799	371.766
3	368.907	368.670	368.500	368.398	368.364
4	365.548	365.308	365.137	365.034	365

Table 48: Thickness d (mm).

0	1	2	3	4	5
1	0.000212	0.000212	0.000213	0.000214	0.000214
2	0.000218	0.000219	0.000219	0.000220	0.000220
3	0.000224	0.000225	0.000226	0.000226	0.000226
4	0.000230	0.000231	0.000232	0.000232	0.000232

Step 10: $\beta = 36°$

Table 49: Nodes angles γ (deg).

0	1	2	3	4	5
1	3.581	2.955	2.409	2.011	1.859
2	3.329	2.631	1.986	1.469	1.250
3	3.174	2.418	1.679	1.001	0.630
4	3.136	2.353	1.569	0.785	0

Table 50: Nodes angles α (deg).

0	1	2	3	4	5
1	37.964	37.919	37.886	37.866	37.859
2	37.359	37.311	37.277	37.256	37.250
3	36.743	36.694	36.658	36.637	36.630
4	36.118	36.066	36.030	36.007	36

Table 51: Nodes distances h (mm).

0	1	2	3	4	5
1	374.548	374.314	374.147	374.047	374.014
2	371.505	371.269	371.101	371	370.966
3	368.504	368.267	368.097	367.995	367.961
4	365.548	365.308	365.137	365.034	365

Table 52: Thickness d (mm).

0	1	2	3	4	5
1	0.000232	0.000233	0.000234	0.000235	0.000235
2	0.000238	0.000239	0.000240	0.000241	0.000241
3	0.000244	0.000246	0.000246	0.000247	0.000247
4	0.000250	0.000252	0.000252	0.000253	0.000253

Step 11: $\beta = 30°$

Table 53: Nodes angles γ (deg).

0	1	2	3	4	5
1	3.663	3.049	2.520	2.140	1.997
2	3.371	2.680	2.048	1.548	1.341
3	3.187	2.433	1.698	1.031	0.675
4	3.136	2.353	1.569	0.785	0

Table 54: Nodes angles α (deg).

0	1	2	3	4	5
1	32.129	32.071	32.030	32.006	31.997
2	31.478	31.418	31.375	31.349	31.341
3	30.817	30.755	30.711	30.684	30.675
4	30.148	30.084	30.037	30.009	30

Table 55: Nodes distances h (mm).

0	1	2	3	4	5
1	373.263	373.028	372.861	372.76	372.726
2	370.641	370.405	370.236	370.135	370.101
3	368.069	367.831	367.662	367.560	367.526
4	365.548	365.308	365.137	365.034	365

Table 56: Thickness d (mm).

0	1	2	3	4	5
1	0.000251	0.000252	0.000253	0.000254	0.000254
2	0.000257	0.000258	0.000259	0.000259	0.000260
3	0.000263	0.000264	0.000265	0.000265	0.000265
4	0.000268	0.000269	0.000270	0.000271	0.000271

Step 12: $\beta = 24°$

Table 57: Nodes angles γ (deg).

0	1	2	3	4	5
1	3.738	3.134	2.617	2.251	2.115
2	3.409	2.724	2.102	1.616	1.418
3	3.199	2.446	1.716	1.057	0.713
4	3.136	2.353	1.569	0.785	0

Table 58: Nodes angles α (deg).

0	1	2	3	4	5
1	26.283	26.210	26.157	26.125	26.115
2	25.594	25.517	25.462	25.429	25.418
3	24.897	24.817	24.759	24.725	24.713
4	24.192	24.108	24.048	24.012	24

Table 59: Nodes distances h (mm).

0	1	2	3	4	5
1	371.892	371.657	371.489	371.388	371.354
2	369.722	369.485	369.316	369.214	369.180
3	367.607	367.368	367.198	367.096	367.062
4	365.548	365.308	365.137	365.034	365

Table 60: Thickness d (mm).

0	1	2	3	4	5
1	0.000268	0.000269	0.000270	0.000270	0.000271
2	0.000273	0.000274	0.000275	0.000276	0.000276
3	0.000278	0.000279	0.000280	0.000281	0.000281
4	0.000283	0.000284	0.000285	0.000286	0.000286

Step 13: $\beta = 18°$

Table 61: Nodes angles γ (deg).

0	1	2	3	4	5
1	3.802	3.205	2.698	2.342	2.210
2	3.443	2.762	2.147	1.672	1.480
3	3.210	2.458	1.730	1.078	0.743
4	3.136	2.353	1.569	0.785	0

Table 62: Nodes angles α (deg).

0	1	2	3	4	5
1	20.436	20.338	20.267	20.224	20.210
2	19.717	19.614	19.540	19.495	19.480
3	18.992	18.884	18.806	18.759	18.743
4	18.262	18.148	18.066	18.017	18

Table 63: Nodes distances h (mm).

0	1	2	3	4	5
1	370.451	370.214	370.046	369.944	369.910
2	368.756	368.518	368.349	368.247	368.213
3	367.121	366.883	366.712	366.610	366.576
4	365.548	365.308	365.137	365.034	365

Table 64: Thickness d (mm).

0	1	2	3	4	5
1	0.000282	0.000283	0.000284	0.000285	0.000285
2	0.000286	0.000288	0.000289	0.000289	0.000289
3	0.000291	0.000292	0.000293	0.000293	0.000294
4	0.000294	0.000296	0.000297	0.000297	0.000298

Step 14: $\beta = 12°$

Table 65: Nodes angles γ (deg).

0	1	2	3	4	5
1	3.855	3.262	2.761	2.411	2.282
2	3.471	2.793	2.182	1.714	1.526
3	3.219	2.468	1.742	1.095	0.765
4	3.136	2.353	1.569	0.785	0

Table 66: Nodes angles α (deg).

0	1	2	3	4	5
1	14.610	14.468	14.365	14.303	14.282
2	13.874	13.723	13.614	13.548	13.526
3	13.137	12.976	12.859	12.789	12.765
4	12.397	12.225	12.101	12.025	12

Table 67: Nodes distances h (mm).

0	1	2	3	4	5
1	368.953	368.716	368.547	368.445	368.411
2	367.754	367.516	367.346	367.243	367.209
3	366.618	366.379	366.209	366.106	366.072
4	365.548	365.308	365.137	365.034	365

Table 68: Thickness d (mm).

0	1	2	3	4	5
1	0.000294	0.000295	0.000296	0.000296	0.000297
2	0.000297	0.000298	0.000299	0.000300	0.000300
3	0.000300	0.000301	0.000302	0.000303	0.000303
4	0.000303	0.000304	0.000305	0.000306	0.000306

Step 15: $\beta = 6°$

Table 69: Nodes angles γ (deg).

0	1	2	3	4	5
1	3.894	3.303	2.805	2.458	2.330
2	3.492	2.815	2.206	1.742	1.556
3	3.227	2.476	1.750	1.105	0.779
4	3.136	2.353	1.569	0.785	0

Table 70: Nodes angles α (deg).

0	1	2	3	4	5
1	8.892	8.651	8.474	8.367	8.330
2	8.174	7.910	7.716	7.596	7.556
3	7.465	7.173	6.957	6.824	6.779
4	6.768	6.443	6.201	6.051	6

Table 71: Nodes distances h (mm).

0	1	2	3	4	5
1	367.416	367.178	367.008	366.905	366.871
2	366.726	366.487	366.317	366.214	366.180
3	366.103	365.864	365.693	365.591	365.556
4	365.548	365.308	365.137	365.034	365

Table 72: Thickness d (mm).

0	1	2	3	4	5
1	0.000302	0.000304	0.000305	0.000305	0.000305
2	0.000304	0.000306	0.000307	0.000307	0.000308
3	0.000306	0.000308	0.000309	0.000309	0.000310
4	0.000308	0.000309	0.000310	0.000311	0.000311

Step 16: $\beta = 0°$

Table 73: Nodes angles γ (deg).

0	1	2	3	4	5
1	3.918	3.326	2.828	2.480	2.353
2	3.506	2.828	2.219	1.754	1.569
3	3.233	2.480	1.754	1.110	0.785
4	3.136	2.353	1.569	0.785	0

Table 74: Nodes angles α (deg).

0	1	2	3	4	5
1	3.918	3.326	2.828	2.480	2.353
2	3.506	2.828	2.219	1.754	1.569
3	3.233	2.480	1.754	1.110	0.785
4	3.136	2.353	1.569	0.785	0

Table 75: Nodes distances h (mm).

0	1	2	3	4	5
1	365.855	365.616	365.445	365.342	365.308
2	365.684	365.445	365.274	365.171	365.137
3	365.582	365.342	365.171	365.068	365.034
4	365.548	365.308	365.137	365.034	365

Table 76: Thickness d (mm).

0	1	2	3	4	5
1	0.000308	0.000309	0.000310	0.000311	0.000311
2	0.000309	0.000310	0.000311	0.000312	0.000312
3	0.000309	0.000311	0.000312	0.000312	0.000313
4	0.000310	0.000311	0.000312	0.000313	0.000313

Step 17: $\beta = -6°$

Table 77: Nodes angles γ (deg).

0	1	2	3	4	5
1	3.927	3.331	2.829	2.479	2.351
2	3.512	2.831	2.219	1.752	1.565
3	3.236	2.483	1.755	1.108	0.782
4	3.136	2.353	1.569	0.785	0

Table 78: Nodes angles α (deg).

0	1	2	3	4	5
1	4.818	4.346	3.974	3.733	3.649
2	5.434	5.022	4.705	4.504	4.435
3	6.088	5.724	5.449	5.277	5.218
4	6.768	6.443	6.201	6.051	6

Table 79: Nodes distances h (mm).

0	1	2	3	4	5
1	364.288	364.047	363.876	363.772	363.738
2	364.639	364.399	364.228	364.125	364.091
3	365.060	364.820	364.648	364.546	364.511
4	365.548	365.308	365.137	365.034	365

Table 80: Thickness d (mm).

0	1	2	3	4	5
1	0.000310	0.000311	0.000313	0.000313	0.000313
2	0.000310	0.000311	0.000312	0.000313	0.000313
3	0.000309	0.000310	0.000311	0.000312	0.000312
4	0.000308	0.000309	0.000310	0.000311	0.000311

Step 18: $\beta = -12°$

Table 81: Nodes angles γ (deg).

0	1	2	3	4	5
1	3.921	3.318	2.809	2.453	2.322
2	3.510	2.825	2.207	1.734	1.544
3	3.238	2.482	1.752	1.101	0.770
4	3.136	2.353	1.569	0.785	0

Table 82: Nodes angles α (deg).

0	1	2	3	4	5
1	10.177	9.962	9.805	9.710	9.678
2	10.916	10.718	10.573	10.486	10.456
3	11.657	11.472	11.338	11.257	11.230
4	12.397	12.225	12.101	12.025	12

Table 83: Nodes distances h (mm).

0	1	2	3	4	5
1	362.730	362.489	362.317	362.213	362.179
2	363.603	363.362	363.190	363.087	363.053
3	364.542	364.302	364.131	364.028	363.993
4	365.548	365.308	365.137	365.034	365

Table 84: Thickness d (mm).

0	1	2	3	4	5
1	0.000309	0.000310	0.000311	0.000312	0.000312
2	0.000307	0.000309	0.000310	0.000310	0.000311
3	0.000305	0.000307	0.000308	0.000308	0.000308
4	0.000303	0.000304	0.000305	0.000306	0.000306

Step 19: $\beta = -18°$

Table 85: Nodes angles γ (deg).

0	1	2	3	4	5
1	3.900	3.288	2.768	2.402	2.267
2	3.502	2.810	2.184	1.701	1.505
3	3.237	2.479	1.745	1.088	0.750
4	3.136	2.353	1.569	0.785	0

Table 86: Nodes angles α (deg).

0	1	2	3	4	5
1	16.042	15.908	15.811	15.753	15.733
2	16.787	16.660	16.568	16.513	16.495
3	17.527	17.407	17.320	17.268	17.250
4	18.262	18.148	18.066	18.017	18

Table 87: Nodes distances h (mm).

0	1	2	3	4	5
1	361.201	360.959	360.786	360.682	360.647
2	362.587	362.345	362.173	362.069	362.035
3	364.036	363.795	363.624	363.520	363.486
4	365.548	365.308	365.137	365.034	365

Table 88: Thickness d (mm).

0	1	2	3	4	5
1	0.000304	0.000306	0.000307	0.000307	0.000307
2	0.000301	0.000303	0.000304	0.000304	0.000304
3	0.000298	0.000299	0.000300	0.000301	0.000301
4	0.000294	0.000296	0.000297	0.000297	0.000298

Step 20: $\beta = -24°$

Table 89: Nodes angles γ (deg).

0	1	2	3	4	5
1	3.865	3.240	2.706	2.327	2.187
2	3.486	2.786	2.149	1.653	1.450
3	3.235	2.474	1.735	1.069	0.721
4	3.136	2.353	1.569	0.785	0

Table 90: Nodes angles α (deg).

0	1	2	3	4	5
1	22.034	21.938	21.869	21.827	21.813
2	22.760	22.669	22.603	22.563	22.550
3	23.480	23.392	23.329	23.292	23.279
4	24.192	24.108	24.048	24.012	24

Table 91: Nodes distances h (mm).

0	1	2	3	4	5
1	359.717	359.474	359.300	359.195	359.160
2	361.602	361.360	361.187	361.083	361.048
3	363.546	363.305	363.133	363.029	362.995
4	365.548	365.308	365.137	365.034	365

Table 92: Thickness d (mm).

0	1	2	3	4	5
1	0.000296	0.000297	0.000298	0.000299	0.000299
2	0.000292	0.000293	0.000294	0.000295	0.000295
3	0.000287	0.000289	0.000290	0.000290	0.000290
4	0.000283	0.000284	0.000285	0.000286	0.000286

Step 21: $\beta = -30°$

Table 93: Nodes angles γ (deg).

0	1	2	3	4	5
1	3.816	3.177	2.626	2.230	2.081
2	3.464	2.755	2.104	1.591	1.378
3	3.231	2.466	1.722	1.045	0.684
4	3.136	2.353	1.569	0.785	0

Table 94: Nodes angles α (deg).

0	1	2	3	4	5
1	28.087	28.014	27.961	27.930	27.919
2	28.783	28.713	28.662	28.632	28.622
3	29.470	29.403	29.354	29.325	29.316
4	30.148	30.084	30.037	30.009	30

Table 95: Nodes distances h (mm).

0	1	2	3	4	5
1	358.295	358.050	357.876	357.771	357.736
2	360.659	360.416	360.243	360.139	360.104
3	363.077	362.836	362.664	362.560	362.526
4	365.548	365.308	365.137	365.034	365

Table 96: Thickness d (mm).

0	1	2	3	4	5
1	0.000284	0.000285	0.000286	0.000287	0.000287
2	0.000279	0.000280	0.000281	0.000282	0.000282
3	0.000274	0.000275	0.000276	0.000276	0.000276
4	0.000268	0.000269	0.000270	0.000271	0.000271

Step 22: $\beta = -36°$

Table 97: Nodes angles γ (deg).

0	1	2	3	4	5
1	3.758	3.101	2.528	2.110	1.951
2	3.438	2.717	2.051	1.517	1.291
3	3.226	2.457	1.707	1.018	0.640
4	3.136	2.353	1.569	0.785	0

Table 98: Nodes angles α (deg).

0	1	2	3	4	5
1	34.182	34.124	34.082	34.057	34.049
2	34.837	34.781	34.742	34.717	34.709
3	35.483	35.429	35.391	35.368	35.360
4	36.118	36.066	36.030	36.007	36

Table 99: Nodes distances h (mm).

0	1	2	3	4	5
1	356.951	356.705	356.530	356.425	356.390
2	359.770	359.526	359.352	359.248	359.213
3	362.636	362.394	362.222	362.118	362.084
4	365.548	365.308	365.137	365.034	365

Table 100: Thickness d (mm).

0	1	2	3	4	5
1	0.000268	0.000270	0.000271	0.000271	0.000271
2	0.000262	0.000264	0.000265	0.000265	0.000265
3	0.000256	0.000258	0.000259	0.000259	0.000259
4	0.000250	0.000252	0.000252	0.000253	0.000253

Step 23: $\beta = -42°$

Table 101: Nodes angles γ (deg).

0	1	2	3	4	5
1	3.691	3.014	2.416	1.971	1.799
2	3.408	2.675	1.991	1.432	1.188
3	3.219	2.447	1.690	0.987	0.589
4	3.136	2.353	1.569	0.785	0

Table 102: Nodes angles α (deg).

0	1	2	3	4	5
1	40.308	40.262	40.228	40.208	40.201
2	40.915	40.870	40.838	40.818	40.812
3	41.510	41.467	41.436	41.418	41.411
4	42.095	42.054	42.024	42.006	42

Table 103: Nodes distances h (mm).

0	1	2	3	4	5
1	355.701	355.455	355.279	355.173	355.138
2	358.943	358.700	358.525	358.421	358.386
3	362.226	361.984	361.812	361.708	361.673
4	365.548	365.308	365.137	365.034	365

Table 104: Thickness d (mm).

0	1	2	3	4	5
1	0.000249	0.000250	0.000251	0.000252	0.000252
2	0.000243	0.000244	0.000245	0.000245	0.000245
3	0.000236	0.000237	0.000238	0.000239	0.000239
4	0.000230	0.000231	0.000232	0.000232	0.000232

Step 24: $\beta = -48°$

Table 105: Nodes angles γ (deg).

0	1	2	3	4	5
1	3.618	2.920	2.293	1.815	1.625
2	3.375	2.630	1.927	1.338	1.072
3	3.212	2.436	1.672	0.954	0.531
4	3.136	2.353	1.569	0.785	0

Table 106: Nodes angles α (deg).

0	1	2	3	4	5
1	46.462	46.424	46.397	46.381	46.375
2	47.011	46.975	46.949	46.933	46.928
3	47.550	47.515	47.490	47.474	47.469
4	48.077	48.043	48.019	48.005	48

Table 107: Nodes distances h (mm).

0	1	2	3	4	5
1	354.560	354.313	354.136	354.030	353.995
2	358.190	357.946	357.771	357.666	357.631
3	361.853	361.611	361.438	361.334	361.300
4	365.548	365.308	365.137	365.034	365

Table 108: Thickness d (mm).

0	1	2	3	4	5
1	0.000227	0.000228	0.000228	0.000229	0.000229
2	0.000220	0.000221	0.000222	0.000222	0.000222
3	0.000213	0.000215	0.000215	0.000216	0.000216
4	0.000207	0.000208	0.000209	0.000209	0.000209

Step 25: $\beta = -54°$

Table 109: Nodes angles γ (deg).

0	1	2	3	4	5
1	3.544	2.823	2.164	1.645	1.431
2	3.343	2.585	1.861	1.239	0.944
3	3.205	2.425	1.654	0.921	0.466
4	3.136	2.353	1.569	0.785	0

Table 110: Nodes angles α (deg).

0	1	2	3	4	5
1	52.639	52.608	52.586	52.573	52.569
2	53.124	53.094	53.073	53.061	53.056
3	53.598	53.570	53.550	53.538	53.534
4	54.062	54.035	54.016	54.004	54

Table 111: Nodes distances h (mm).

0	1	2	3	4	5
1	353.541	353.293	353.117	353.010	352.975
2	357.518	357.273	357.098	356.993	356.958
3	361.521	361.278	361.105	361.002	360.967
4	365.548	365.308	365.137	365.034	365

Table 112: Thickness d (mm).

0	1	2	3	4	5
1	0.000201	0.000202	0.000203	0.000203	0.000203
2	0.000194	0.000195	0.000196	0.000196	0.000196
3	0.000188	0.000189	0.000190	0.000190	0.000190
4	0.000182	0.000183	0.000183	0.000184	0.000184

Step 26: $\beta = -60°$

Table 113: Nodes angles γ (deg).

0	1	2	3	4	5
1	3.472	2.728	2.034	1.467	1.221
2	3.311	2.541	1.797	1.137	0.804
3	3.199	2.414	1.637	0.888	0.397
4	3.136	2.353	1.569	0.785	0

Table 114: Nodes angles α (deg).

0	1	2	3	4	5
1	58.835	58.811	58.793	58.783	58.779
2	59.250	59.226	59.210	59.199	59.196
3	59.654	59.632	59.616	59.606	59.603
4	60.050	60.028	60.012	60.003	60

Table 115: Nodes distances h (mm).

0	1	2	3	4	5
1	352.657	352.409	352.231	352.125	352.090
2	356.936	356.690	356.515	356.410	356.375
3	361.233	360.990	360.817	360.713	360.679
4	365.548	365.308	365.137	365.034	365

Table 116: Thickness d (mm).

0	1	2	3	4	5
1	0.000172	0.000173	0.000174	0.000174	0.000174
2	0.000166	0.000167	0.000168	0.000168	0.000168
3	0.000160	0.000161	0.000162	0.000162	0.000162
4	0.000155	0.000156	0.000156	0.000156	0.000156

Step 27: $\beta = -66°$

Table 117: Nodes angles γ (deg).

0	1	2	3	4	5
1	3.406	2.639	1.910	1.286	0.995
2	3.282	2.501	1.738	1.038	0.655
3	3.192	2.405	1.622	0.858	0.323
4	3.136	2.353	1.569	0.785	0

Table 118: Nodes angles α (deg).

0	1	2	3	4	5
1	65.048	65.029	65.016	65.008	65.005
2	65.387	65.368	65.356	65.348	65.345
3	65.716	65.699	65.687	65.679	65.677
4	66.038	66.022	66.010	66.002	66

Table 119: Nodes distances h (mm).

0	1	2	3	4	5
1	351.919	351.670	351.492	351.385	351.350
2	356.449	356.204	356.028	355.923	355.888
3	360.992	360.750	360.577	360.473	360.438
4	365.548	365.308	365.137	365.034	365

Table 120: Thickness d (mm).

0	1	2	3	4	5
1	0.000141	0.000142	0.000142	0.000142	0.000143
2	0.000136	0.000136	0.000137	0.000137	0.000137
3	0.000131	0.000131	0.000132	0.000132	0.000132
4	0.000126	0.000126	0.000127	0.000127	0.000127

Step 28: $\beta = -72°$

Table 121: Nodes angles γ (deg).

0	1	2	3	4	5
1	3.350	2.563	1.800	1.114	0.757
2	3.258	2.467	1.686	0.947	0.498
3	3.187	2.397	1.609	0.832	0.246
4	3.136	2.353	1.569	0.785	0

Table 122: Nodes angles α (deg).

0	1	2	3	4	5
1	71.274	71.261	71.251	71.245	71.243
2	71.532	71.519	71.510	71.504	71.502
3	71.783	71.771	71.762	71.756	71.754
4	72.028	72.016	72.007	72.002	72

Table 123: Nodes distances h (mm).

0	1	2	3	4	5
1	351.335	351.085	350.907	350.800	350.765
2	356.065	355.819	355.643	355.538	355.503
3	360.803	360.560	360.387	360.283	360.248
4	365.548	365.308	365.137	365.034	365

Table 124: Thickness d (mm).

0	1	2	3	4	5
1	0.000108	0.000108	0.000109	0.000109	0.000109
2	0.000103	0.000104	0.000104	0.000105	0.000105
3	9.95E-05	9.99E-05	0.000100	0.000100	0.000101
4	9.57E-05	9.61E-05	9.64E-05	9.66E-05	9.67E-05

Step 29: $\beta = -78°$

Table 125: Nodes angles γ (deg).

0	1	2	3	4	5
1	3.307	2.504	1.713	0.964	0.510
2	3.240	2.441	1.647	0.873	0.335
3	3.183	2.391	1.599	0.812	0.165
4	3.136	2.353	1.569	0.785	0

Table 126: Nodes angles α (deg).

0	1	2	3	4	5
1	77.511	77.502	77.495	77.491	77.490
2	77.684	77.676	77.670	77.666	77.665
3	77.854	77.845	77.839	77.836	77.835
4	78.018	78.010	78.005	78.001	78

Table 127: Nodes distances h (mm).

0	1	2	3	4	5
1	350.912	350.663	350.484	350.377	350.342
2	355.787	355.541	355.365	355.260	355.225
3	360.666	360.423	360.250	360.145	360.111
4	365.548	365.308	365.137	365.034	365

Table 128: Thickness d (mm).

0	1	2	3	4	5
1	7.27E-05	7.31E-05	7.33E-05	7.35E-05	7.35E-05
2	6.98E-05	7.01E-05	7.04E-05	7.05E-05	7.06E-05
3	6.70E-05	6.73E-05	6.75E-05	6.77E-05	6.77E-05
4	6.44E-05	6.47E-05	6.49E-05	6.50E-05	6.50E-05

Step 30: $\beta = -84°$

Table 129: Nodes angles γ (deg).

0	1	2	3	4	5
1	3.280	2.467	1.656	0.858	0.257
2	3.228	2.425	1.622	0.824	0.169
3	3.181	2.387	1.593	0.800	0.083
4	3.136	2.353	1.569	0.785	0

Table 130: Nodes angles α (deg).

0	1	2	3	4	5
1	83.754	83.749	83.746	83.744	83.743
2	83.841	83.837	83.834	83.832	83.831
3	83.926	83.922	83.919	83.917	83.917
4	84.009	84.005	84.002	84.001	84

Table 131: Nodes distances h (mm).

0	1	2	3	4	5
1	350.657	350.407	350.228	350.121	350.086
2	355.619	355.373	355.197	355.092	355.056
3	360.583	360.340	360.167	360.062	360.028
4	365.548	365.308	365.137	365.034	365

Table 132: Thickness d (mm).

0	1	2	3	4	5
1	3.66E-05	3.68E-05	3.70E-05	3.70E-05	3.71E-05
2	3.51E-05	3.53E-05	3.54E-05	3.55E-05	3.55E-05
3	3.37E-05	3.39E-05	3.40E-05	3.41E-05	3.41E-05
4	3.24E-05	3.25E-05	3.26E-05	3.27E-05	3.27E-05